INFRARED VIDICON OBSERVATIONS OF EXPLODING BALLOON EVENTS

F. Alyea, et al

General Electric Company

Prepared for:

Defense Advanced Research Projects Agency
Rome Air Development Center

May 1975

RADC-TR-74-179
Final Technical Report
May 1974

INFRARED VIDICON OBSERVATIONS OF EXPLODING BALLOON EVENTS

General Electric Co/Space Sciences Lab

Sponsored By
Defense Advanced Research Projects Agency
ARPA Order No. 1649

Approved for public release;
distribution unlimited.

Rome Air Development Center
Air Force Systems Command
Griffiss Air Force Base, New York 13441

UNCLASSIFIED

SECURITY CLASSIFICATION OF THIS PAGE *(When Data Entered)*

REPORT DOCUMENTATION PAGE

READ INSTRUCTIONS BEFORE COMPLETING FORM

1. REPORT NUMBER: RADC-TR-75-139	2. GOVT ACCESSION NO.
3. RECIPIENT'S CATALOG NUMBER: AD-A011 774	
4. TITLE *(and Subtitle)*: INFRARED VIDICON OBSERVATIONS OF EXPLODING BALLOON EVENTS	5. TYPE OF REPORT & PERIOD COVERED: Final Technical Report April 1974 - February 1975
	6. PERFORMING ORG. REPORT NUMBER
7. AUTHOR(s): Dr. F. Alyea Mr. R. Culatsi	8. CONTRACT OR GRANT NUMBER(s): F30602-74-C-0049
9. PERFORMING ORGANIZATION NAME AND ADDRESS: General Electric Co/Space Sciences Lab P O Box 8555 Philadelphia PA 19101	10. PROGRAM ELEMENT, PROJECT, TASK AREA & WORK UNIT NUMBERS: 62301E 16490703
11. CONTROLLING OFFICE NAME AND ADDRESS: Defense Advanced Research Projects Agency 1400 Wilson Blvd Arlington VA 22209	12. REPORT DATE: May 1975
	13. NUMBER OF PAGES: 68
14. MONITORING AGENCY NAME & ADDRESS *(if different from Controlling Office)*: Rome Air Development Center (OCSE) Griffiss AFB NY 13441	15. SECURITY CLASS. *(of this report)*: UNCLASSIFIED
	15a. DECLASSIFICATION DOWNGRADING SCHEDULE: N/A

16. DISTRIBUTION STATEMENT *(of this Report)*

Approved for public release; distribution unlimited.

17. DISTRIBUTION STATEMENT *(of the abstract entered in Block 20, if different from Report)*

Same

18. SUPPLEMENTARY NOTES

RADC Project Engineer:
Joseph J. Simons (OCSE)
AC 315 330-3141

19. KEY WORDS *(Continue on reverse side if necessary and identify by block number)*

Infrared Emissions
Exploding Methane/Oxygen Balloons
Simulation Techniques

PRICES SUBJECT TO CHANGE

20. ABSTRACT *(Continue on reverse side if necessary and identify by block number)*

The Air Force Weapons Laboratory conducted a series of experiments as part of Project GEST (Gas Explosive Simulation Technique) to evaluate the flow characteristics of fireballs resulting from balloon explosions. A primary diagnostic for these events was an infrared vidicon sensor system operated by the General Electric Company, Space Sciences Laboratory (GE-SSL) under the sponsorship of the Defense Advanced Research Projects Agency (DARPA). This report presents the results of these diagnostic experiments. (Cont'd)

DD FORM 1 JAN 73 1473 EDITION OF 1 NOV 65 IS OBSOLETE

UNCLASSIFIED

SECURITY CLASSIFICATION OF THIS PAGE *(When Data Entered)*

The tests were conducted at Kirtland Air Force Base, New Mexico and consisted of detonating tethered balloons filled with an explosive mixture of CH_4 and O_2. Predictions of the fireball flow field (Reference 1) and of the resulting optical signature (Reference 2) showed that the optimum wavelength for observation was 3.3μ based on a trade-off between vidicon characteristics, atmospheric transmission and spectral properties of the debris. Further, the expected dynamic range of the signature was 1×10^5. For these reasons, the vidicon sensor system which was deployed consisted of two infrared vidicon cameras equipped with narrow band spectral bandpass filters. Removable aperture stops provided the desired dynamic range.

Initial results of the experiments have been previously documented (Reference 3), while the present report centers on quantitative data reduction. The derived results include metric information such as shape, size, and altitude behavior of the debris and iso-intensity contours presented as a function of time.

INFRARED VIDICON OBSERVATIONS OF EXPLODING BALLOON EVENTS

Dr. F. Alyea
Mr. R. Gulatsi

Contractor: General Electric Co/Space Sciences Lab
Contract Number: F30602-74-C-0049
Effective Date of Contract: 7 December 1973
Contract Expiration Date: 7 March 1975
Amount of Contract: $155,000.00
Program Code Number: 4E20
Period of Report Covered: Apr 74 - Feb 75

Principal Investigator: Dr. F. Alyea
Phone: 215 962-6038

Project Engineer: Joseph J. Simons
Phone: 315 330-3141

Approved for public release;
distribution unlimited.

This research was supported by the Defense Advanced Research Projects Agency of the Department of Defense and was monitored by Joseph J. Simons (OCSE) Griffiss AFB NY 13441.

TABLE OF CONTENTS

LIST OF FIGURES

LIST OF FIGURES (CONT'D.)

PAGE

LIST OF TABLES

I. INTRODUCTION

The Air Force Weapons Laboratory conducted a series of experiments as part of Project GEST (Gas Explosive Simulation Technique) to evaluate the flow characteristics of fireballs resulting from balloon explosions. A primary diagnostic for these events was an infrared vidicon sensor system operated by the General Electric Company, Space Sciences Laboratory (GE-SSL) under the sponsorship of the Defense Advanced Research Projects Agency (DARPA). This report presents the results of these diagnostic experiments.

The tests were conducted at Kirtland Air Force Base, New Mexico and consisted of detonating tethered balloons filled with an explosive mixture of CH_4 and O_2. Predictions of the fireball flow field (Reference 1) and of the resulting optical signature (Reference 2) showed that the optimum wavelength for observation was 3.3μ based on a trade-off between vidicon characteristics, atmospheric transmission and spectral properties of the debris. Further, the expected dynamic range of the signature was 1×10^5. For these reasons, the vidicon sensor system which was deployed consisted of two infrared vidicon cameras equipped with narrow band spectral bandpass filters. Removable aperture stops provided the desired dynamic range.

Initial results of the experiments have been previously documented (Reference 3), while the present report centers on quantitative data reduction. The derived results include metric information such as shape, size, and altitude behavior of the debris and iso-intensity contours presented as a function of time.

II. EXPERIMENT DESCRIPTION

II.1 Test Geometry

The Project GEST tests observed by the GE vidicons took place on 11 December 1973 at 1630 hrs. GMT (0930 MST) and 13 December 1973 at 1500 hrs. GMT (0800 MST) at the Old Sandia Overhead Cable Site in Mandera Canyon, Kirtland AFB. Thirty-two foot balloons were filled with a detonable mixture of methane and oxygen and suspended from a horizontal steel cable which was anchored in the adjoining hillsides. At detonation, the balloon was elevated to a height of 130 ft. above the canyon floor. For purposes of boresighting the vidicons, the cable was provided with an infrared boresight light at the center of the cable over the suspension point of the balloon. Distance from the vidicon site to the balloon location was 3,416 ft. (see Figure 1.)

II.2 Instrumentation

Two infrared vidicon cameras were employed for the measurements. The cameras had identical spectral bandpass characteristics, but had predicted dynamic ranges which were stacked in such a way as to maximize the dynamic range of source intensities which could be observed.

The camera systems have the following basic characteristics:

System #1 (Referred to as the Belvoir Camera)

Vidicon:	General Electric Z7934R Reticulated Ge:Cu Vidicon.
Optics:	10-inch focal length f/2.
Cryogenics:	Pressure dewar with controlled LN_2 feed to sensor.
Unvignetted Field-of-View:	4.1^{o} x 4.1^{o}.
Frame Rate:	Standard 30 frame per second television raster.
Camera Chain:	Infrared vidicon field camera built for DARPA by General Electric under Contract DA-44-009-AMC (520X). (Supplied as GFE by U.S. Army Night Vision Laboratory, Fort Belvoir, Virginia.)
Data Recorder:	Ampex VR 7000 video recorder.
Displays:	C-scope monitor.
Calibration Source:	Barnes Engineering Co., Model 11-140T Blackbody (12 inch x 12 inch radiating area).

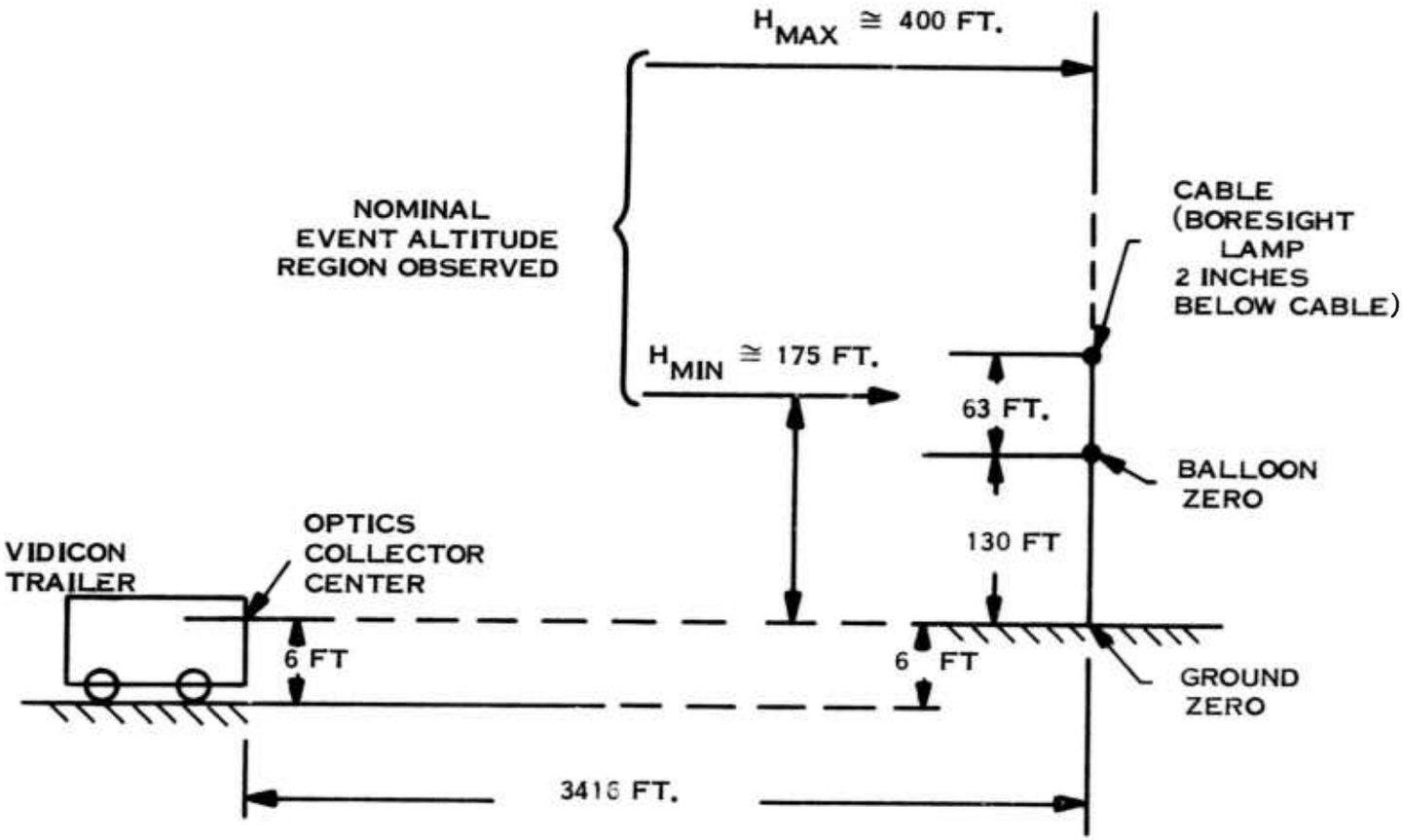

FIGURE 1. MEASUREMENT GEOMETRY

System #2 (Referred to as the NRL Camera)

Vidicon:	General Electric Z7876 Ge:Cu Vidicon.
Optics:	4-inch focal length f/1.
Cryogenics:	Hand-fill LN_2 to vidicon tube.
Unvignetted Field-of-View:	5.0^{o} x 5.0^{o}.
Frame Rate:	Standard 30 frame per second television raster.
Camera Chain:	Infrared field camera built for Naval Research Laboratory (NRL) by General Electric under Contract N00014-70-C-0340. (Supplied as GFE by NRL.)
Data Recorder:	Same as Camera #1.
Displays:	Same as Camera #1.
Calibration Source:	Same as Camera #1.

Both cameras had identical spectral bandpass filters with the transmission curve given in Figure 2. The intent of this wavelength selection was to observe hot bands of H_2O without the complicating effects of other debris species.

In order to extend the useful dynamic range of the cameras, each was fitted with a hand-held, removable aperture stop consisting of a metal plate in which a small hole was drilled. The Belvoir camera stop consisted of a 0.138" diameter hole, which, when placed over the five inch diameter optics resulted in a net transmission of 0.076%, or an f/72 optical system. Similarly, the four inch NRL lens was stopped with a 0.66" aperture, giving a transmission of 2.7%, or an f/6 optic. Figure 3 shows the expected dynamic range configuration.

II.3 Radiometric Calibration

The vidicon radiometric transfer function can be written as:

$$S/N = \frac{T_o(\lambda)_{ref} T_f(\lambda)_{ref}}{4F^2 \; NEH(\lambda)_{ref}} \int \Delta N_{\lambda_{(c)}} R^1(\lambda) \; T_a(\lambda)_c \; T_o^1(\lambda) \; T_f^1(\lambda) \; d\lambda$$

where:

$T_o(\lambda)_{ref}$ = absolute optics transmission at λ_{ref} (filter center wavelength).

$T_f(\lambda)_{ref}$ = absolute spectral filter transmission at λ_{ref}.

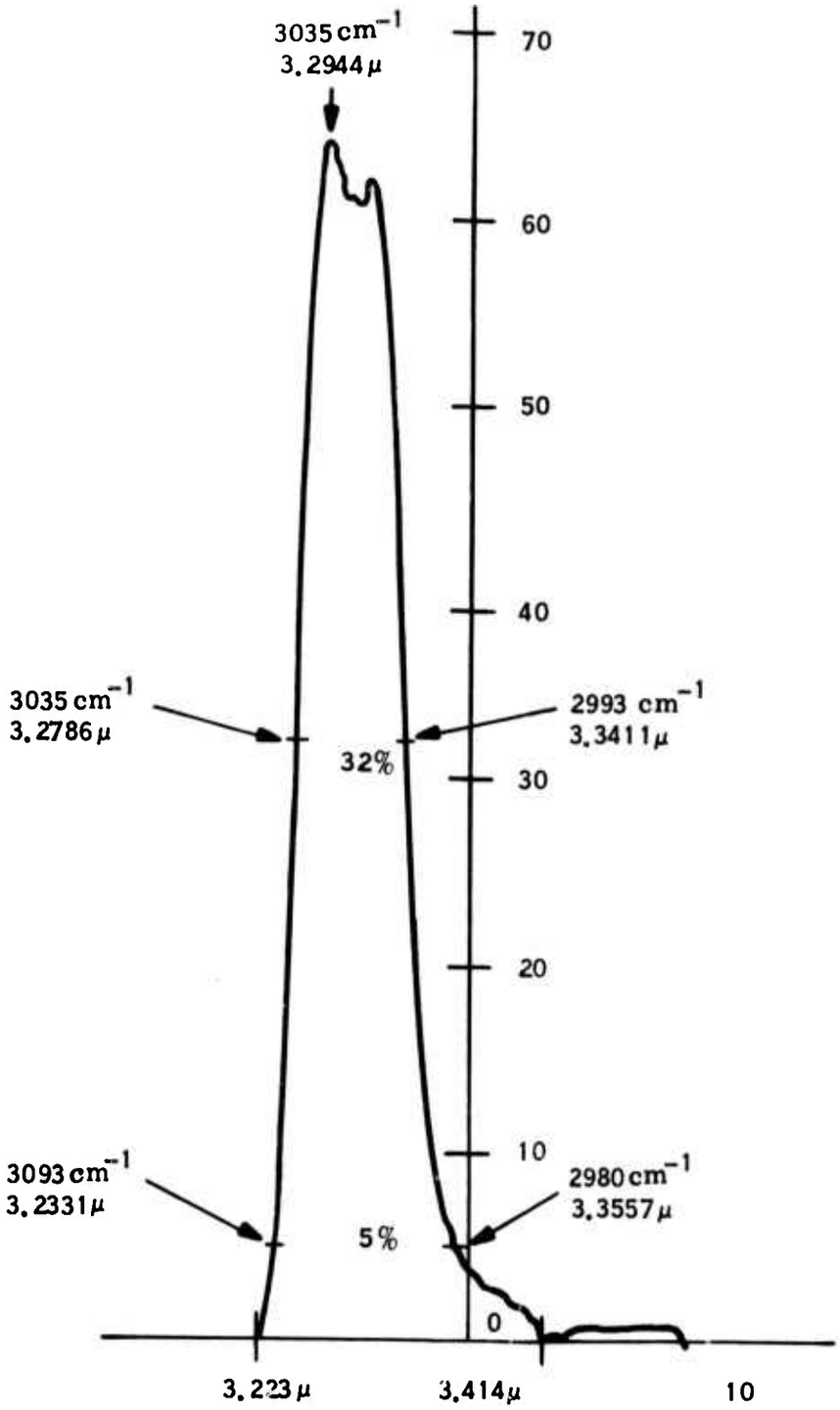

FIGURE 2. VIDICON SPECTRAL FILTER TRANSMISSION CALIBRATION CURVE

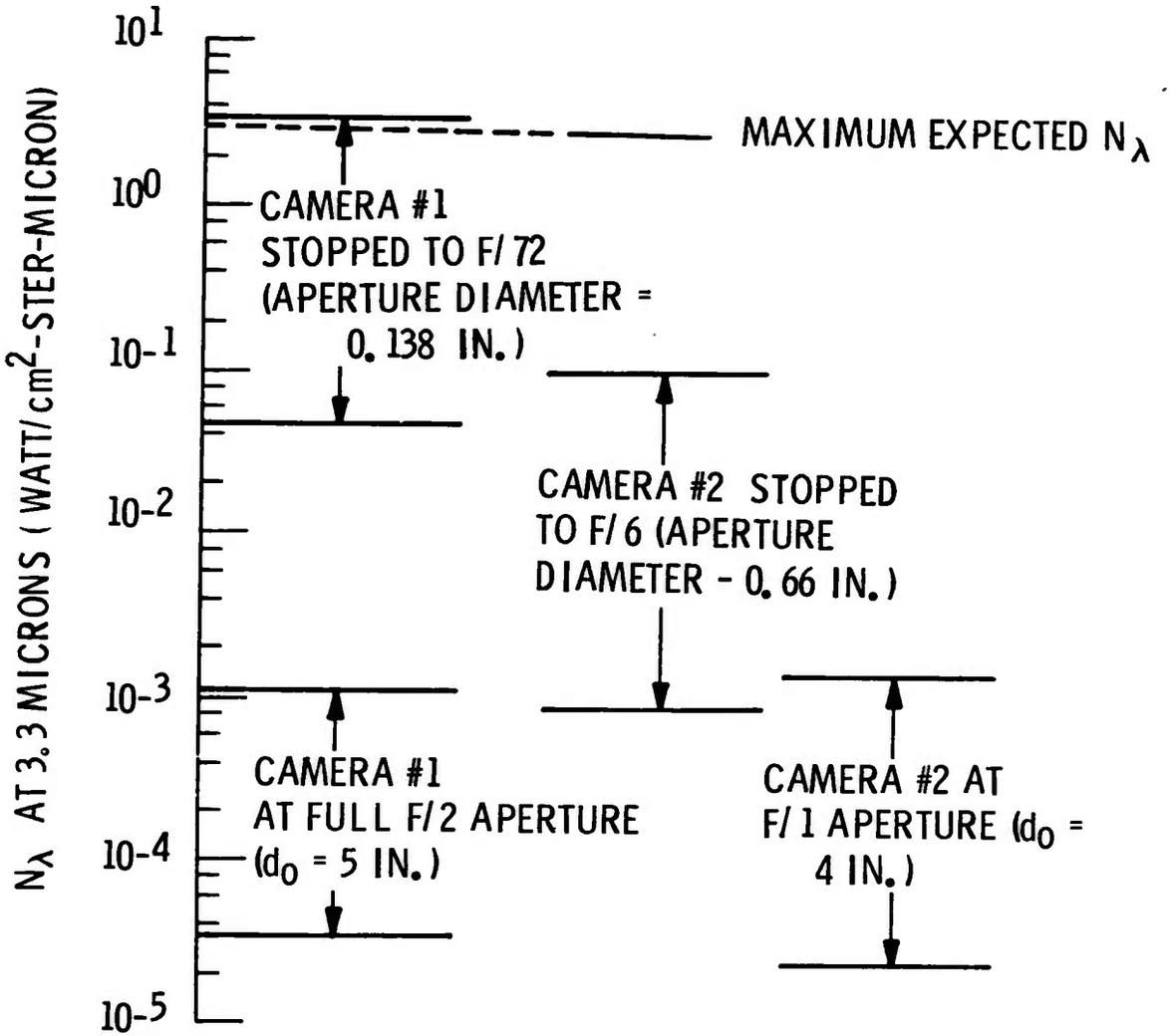

FIGURE 3. MEASUREMENT DYNAMIC RANGE

$T_o^1(\lambda)$ and $T_f^1(\lambda)$ are relative optics and filter transmission (normalized to the absolute value at λ_{ref}).

$T_a(\lambda)_c$ = atmospheric spectral transmission over calibration path.

$\Delta N_{\lambda_{(c)}}$ = differential spectral radiance of calibration source above adjacent background, watt-cm^{-2}-ster-$micron^{-1}$. At the source temperatures typically used in the calibration, $\Delta N_{\lambda_{(c)}} \approx N_{\lambda_{(c)}}$, i.e., the background radiance is negligible.

$R^1(\lambda)$ = vidicon relative spectral responsivity normalized to the absolute value of the vidicon responsivity at λ_{ref}.

$NEH(\lambda)_{ref}$ = retina noise equivalent irradiance at λ_{ref}.

λ_{ref} = center of effective system passband.

F = F-number of optics.

In the above equation, the quantity:

$$\frac{T_o(\lambda)_{ref} T_f(\lambda)_{ref}}{4F^2 \quad NEH(\lambda)_{ref}}$$

is an instrument constant, i.e., for operation in the vidicon linear dynamic range:

$$S/N = C \int \Delta N_{\lambda_{(c)}} R^1(\lambda)\ T_a(\lambda)\ T_o^1(\lambda)\ T_f^1(\lambda)\ d\lambda \qquad (1)$$

The instrument constant, C, was measured following the test of 13 December 1973. The procedure consisted of observing the radiance of a 12 inch x 12 inch blackbody source located a distance of approximately 50 feet from the vidicon cameras and evaluating the calibration integrals (Reference 2).

The results for the calibration of the Belvoir camera are shown in Figure 4. These differ from coinciding predicted performance and pre-mission laboratory calibration in that the observed threshold at S/N = 1 is in the region of three times that noted in predicted performance/laboratory calibration. Dynamic range is similarly decreased. This is primarily due to increased noise noted in the video recordings taken at the field site.

No calibration data plot is presented for the NRL camera since the vidicon tube employed (the only available tube, a seven-year old Z7876) commenced "going soft" after arrival at the field site. The result was an

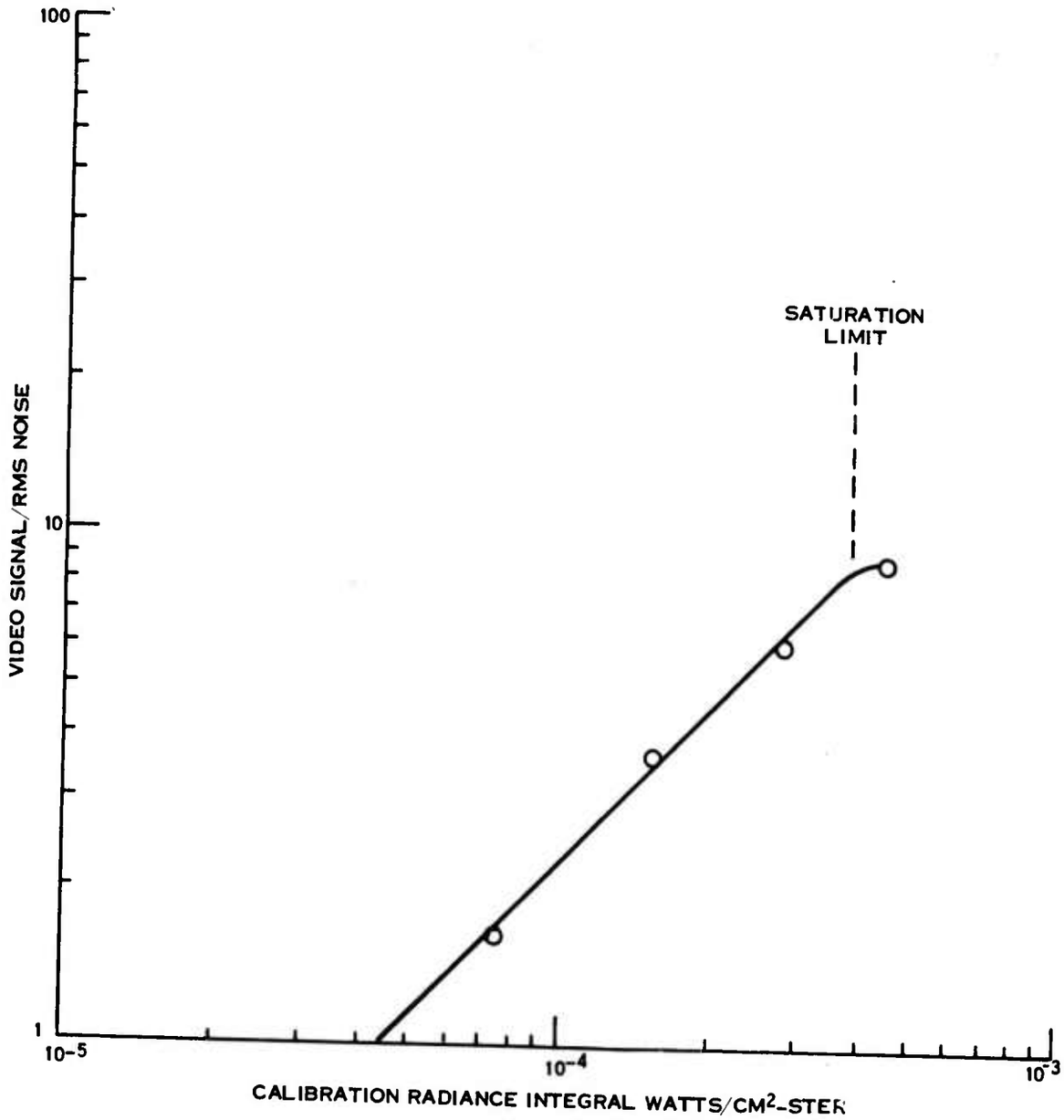

FIGURE 4. BELVOIR CAMERA POST-MISSION CALIBRATION

order of magnitude increase in noise-equivalent source radiance and a drastic reduction in dynamic range. Noise-equivalent source radiance of 1.62×10^{-4} watt/cm^2-ster was noted from the calibration data.

II.4 Instrument Performance

The best data were obtained by the Belvoir camera on the 13 December event. No data were obtained by this camera on the 11 December event since an on-cable boresite lamp of sufficient intensity was not provided for optical alignment on that date. On the 13 December event, the Belvoir camera observed the event from detonation to about T + 9.5 seconds. However, some data in the middle region was saturated, as predicted by the experiment plan.

The NRL camera obtained 5 seconds of data on both the 11 December and 13 December events. (Unlike the Belvoir camera, an attempt at approximate optical alignment in the absence of a boresite lamp on 11 December was successful.) Despite the vidicon degradation discussed in the previous section, the NRL data is of adequate quality to allow identification of source characteristics at the threshold intensity in question, about equivalent to a 465°K blackbody.

III. EXPERIMENT RESULTS

Metric information describing the size, shape and position of the debris of the 13 December balloon explosion has been derived directly from a TV display of the recorded video tapes. The measurements were analyzed using a video tape display station which presents a single video frame on a TV monitor, or C-scope, and also permits the video amplitude of a single TV scan line to be shown on an oscilloscope or A-scope.

Figure 5 shows A and C-scope photographs for a typical data frame. The TV scan line which has been selected for display on the A-scope is indicated by a white marker pulse on the C-scope and shown as a pulse on the lower trace of the A-scope. The vidicon tube in the Belvoir camera had a major blemish on its retina which shows up as a constant spot to the right of the frame center. The sample data frame shows the rising cloud at a time when part of the signal is above the saturation limit of the vidicon. At saturation, the vidicon exhibits a reversal effect, so that the saturated portion of the image appears black on the C-scope, this correlates with minima in the A-scope video signal level.

Quantitative measurements of the cloud geometry have been made directly from the A and C-scope displays using the known experimental geometry (Figure 1) and field-of-view calibrations (Reference 3). Figure 6 presents sample data frames while the metric results are given in Figures 7-14 where the measured quantity is defined schematically on each figure.

Prior to discussing the results, it is cautioned that size measurements of this nature depend on camera threshold; 435°K and 465°K equivalent source intensity for the Belvoir (System #1) and NRL (System #2) cameras, respectively. Thus, measurements from the two cameras should be and are consistent (see Figures 10-14), but comparisons with other data and with theoretical predictions of cloud geometry must be based on identical threshold intensities.

Figure 6 presents the evolution of the flow associated with the balloon explosion. The first frame, corresponding to an event time of T + 0.2 seconds shows the cloud entering the bottom of the camera field-of-view. At this time, the aperture stop was in place and the intensity is attenuated by a factor of 7.7×10^{-4}. The next two frames, at times T + 1.1 and 1.6

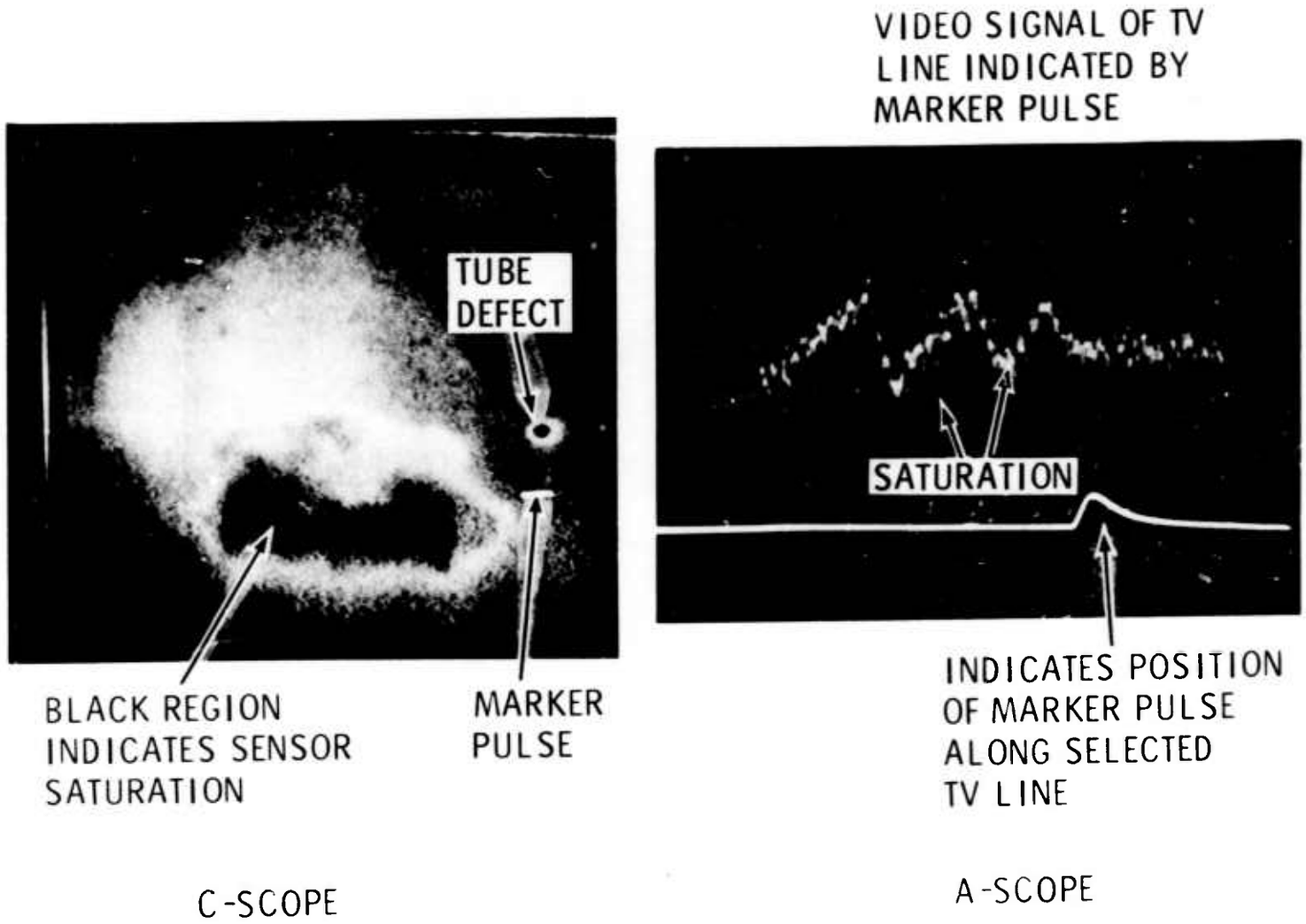

FIGURE 5. SAMPLE VIDICON DATA FRAME

PART 1

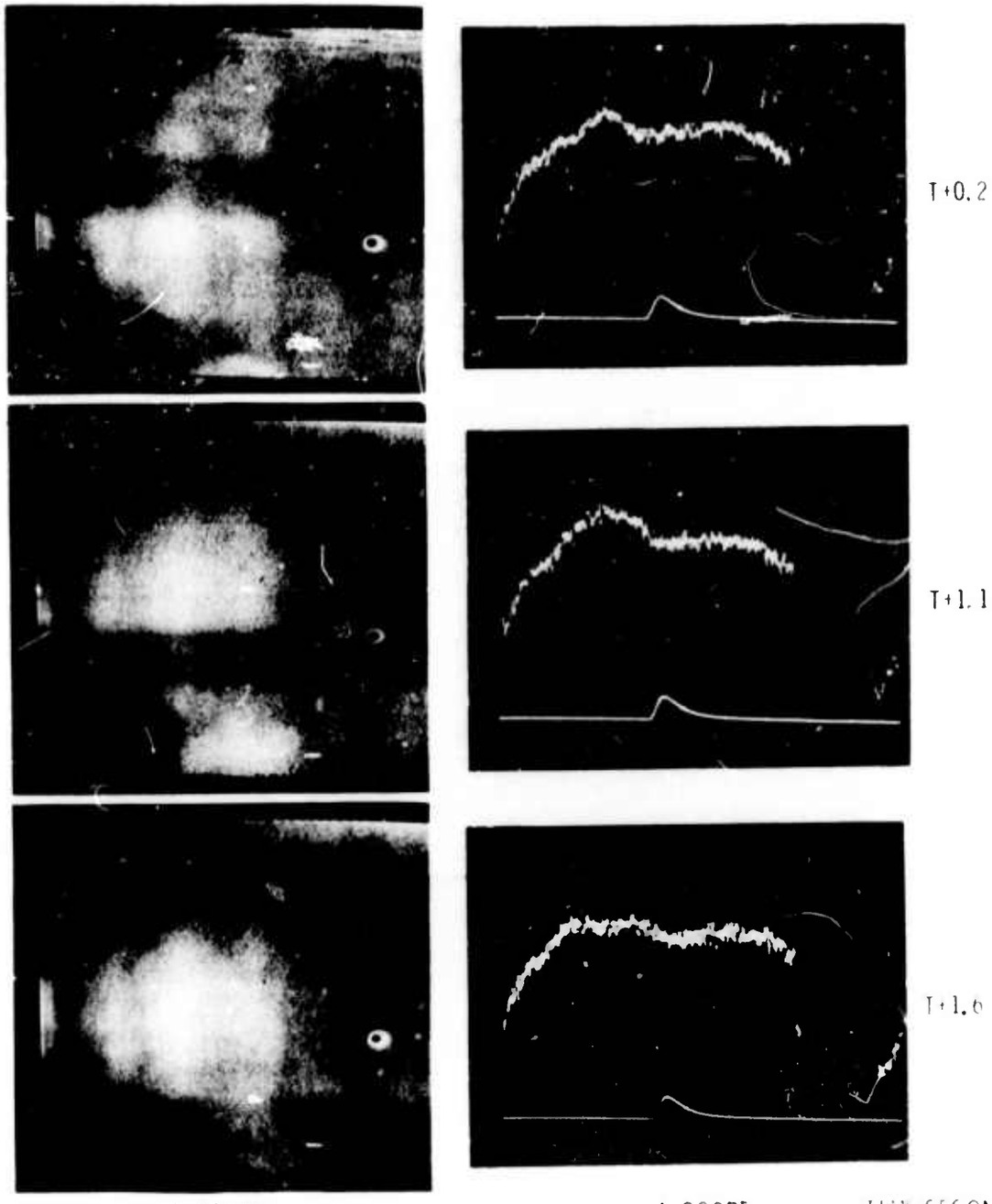

APERTURE STOP IN PLACE

FIGURE 6. PART 1. BELVOIR CAMERA DATA FRAMES

PART 2

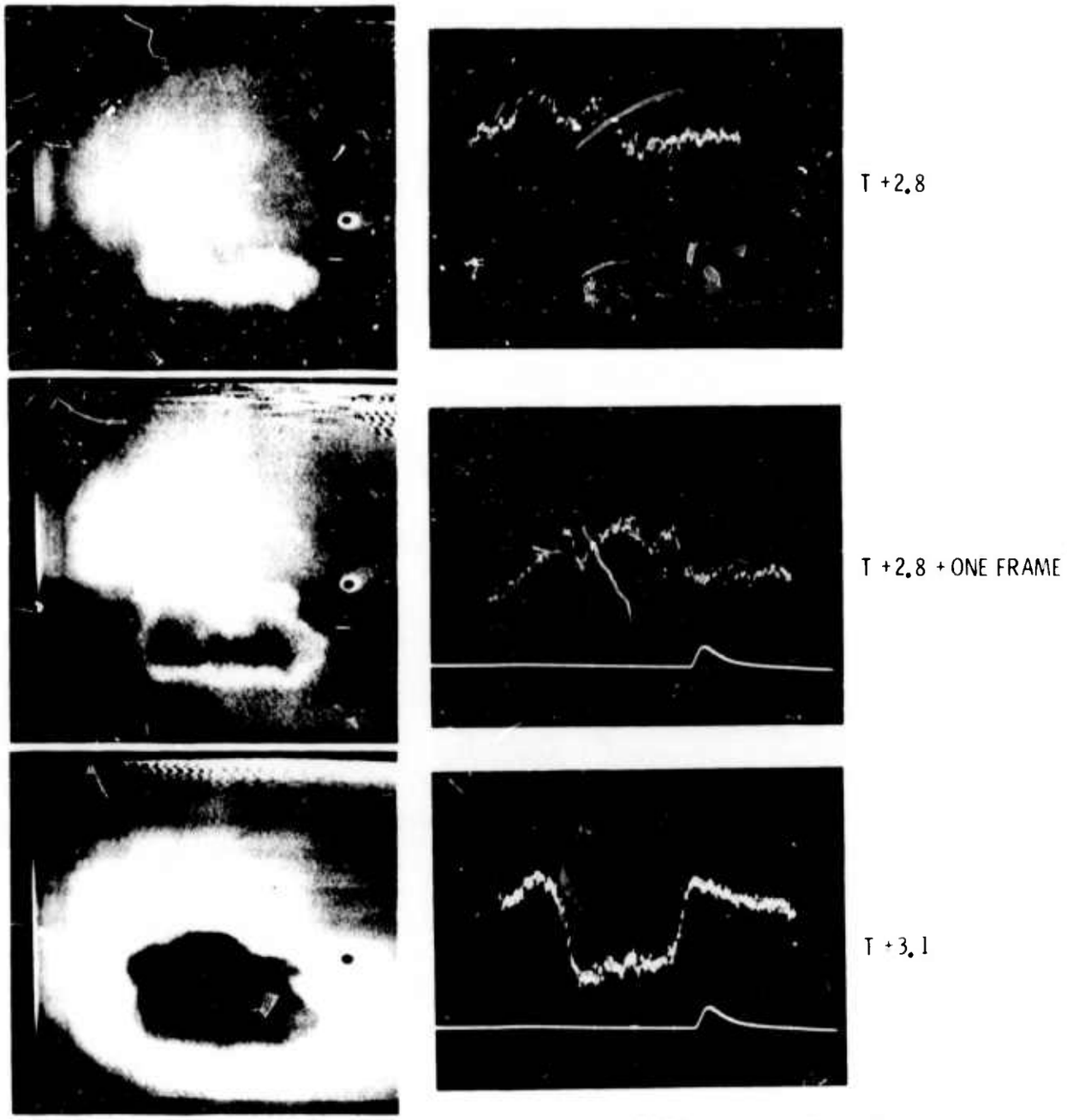

FIGURE 6. PART 2. BELVOIR CAMERA DATA FRAMES

PART 3

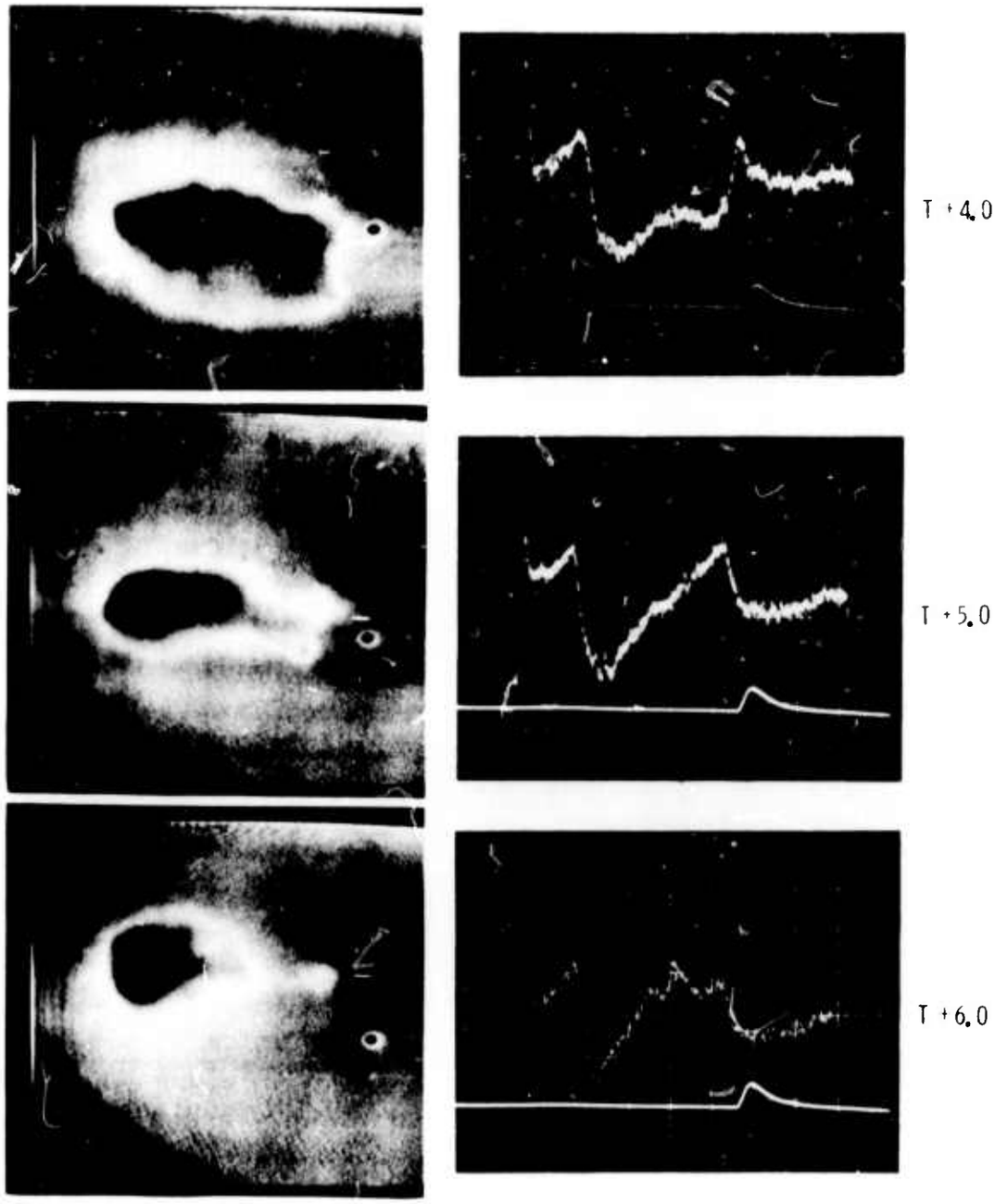

FIGURE 6. PART 3. BELVOIR CAMERA DATA FRAMES

PART 4

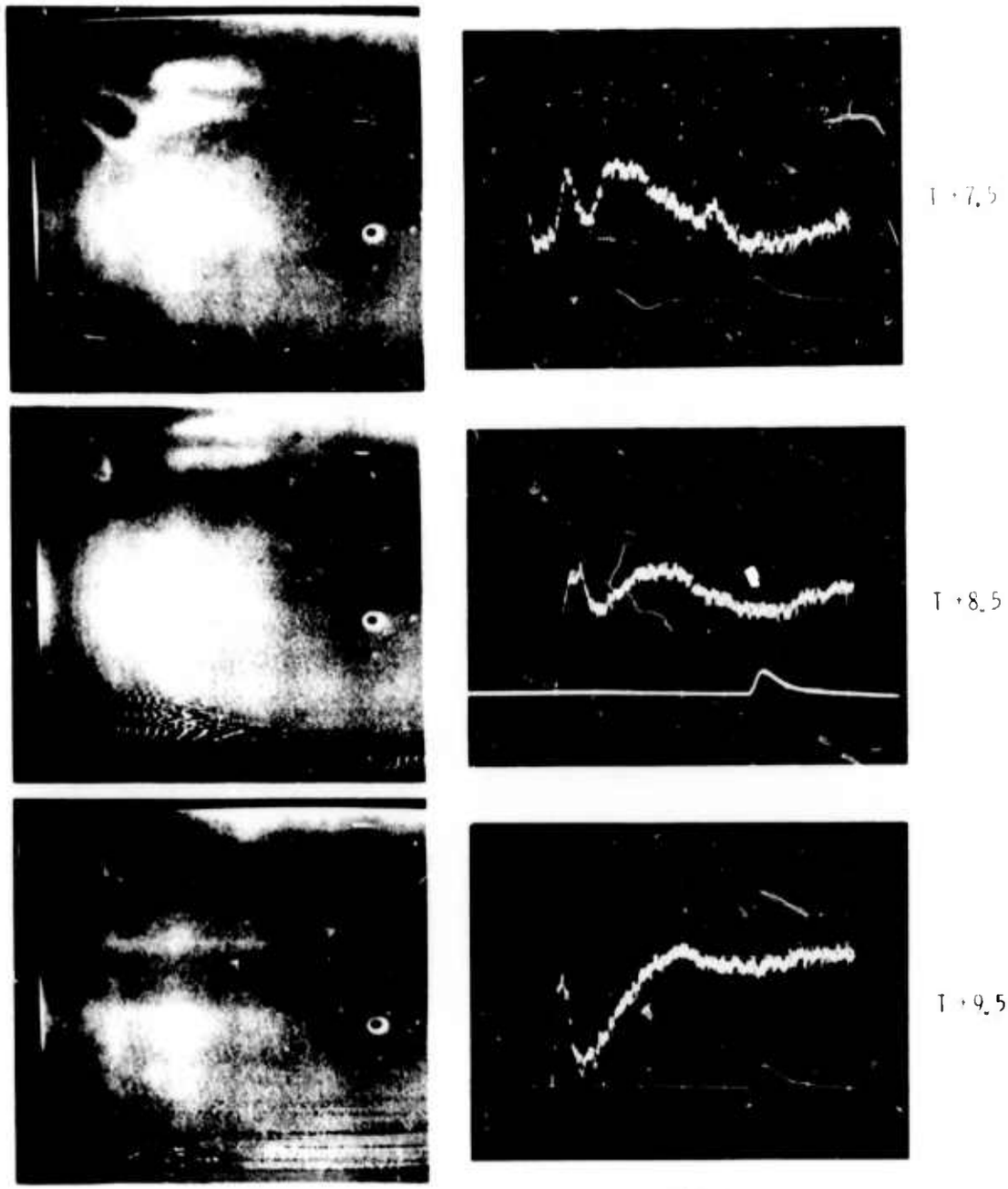

C-SCOPE A-SCOPE TIME (SECONDS)

APERTURE STOP FULLY REMOVED

FIGURE 6. PART 4. BELVOIR CAMERA DATA FRAMES

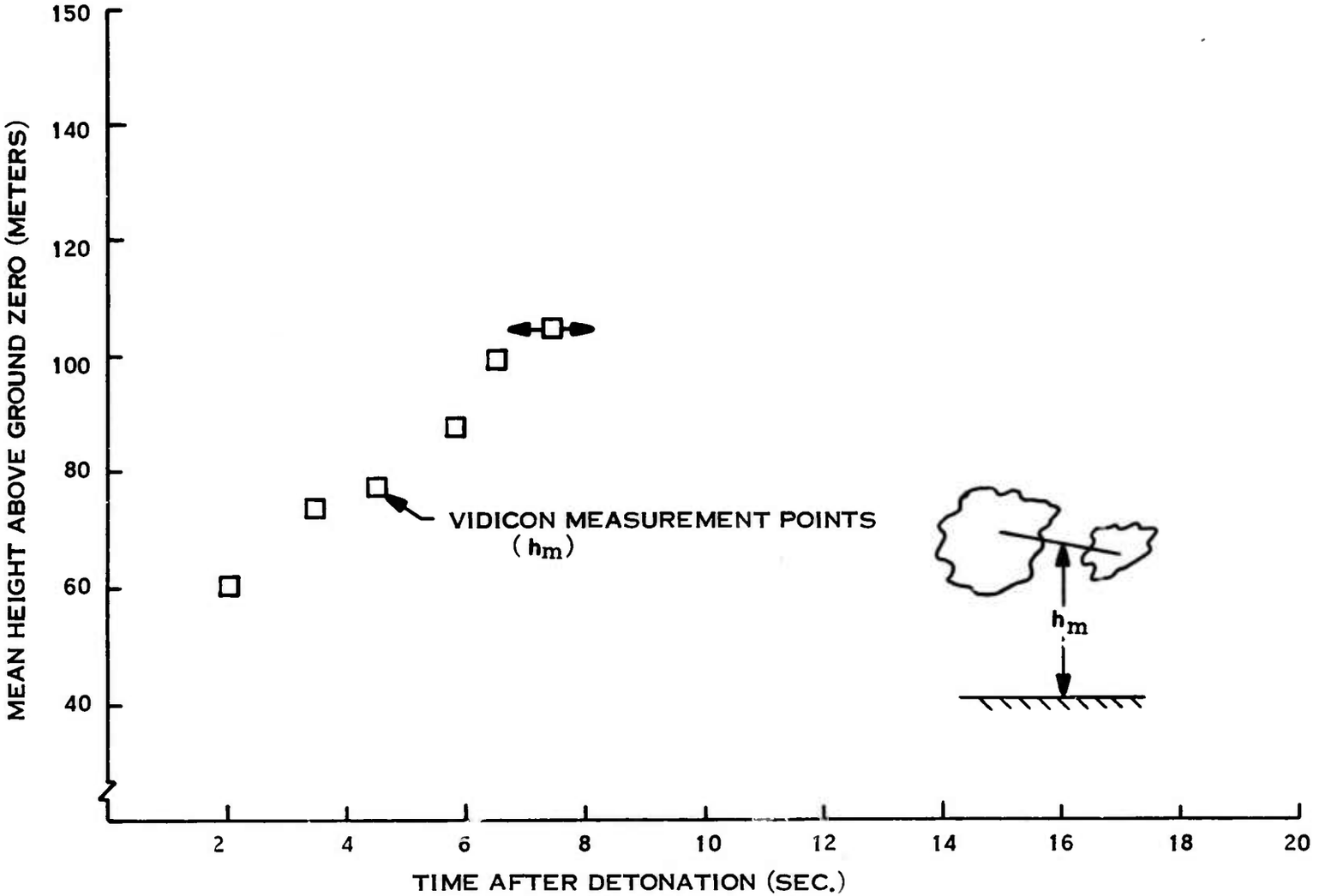

FIGURE 7. CLOUD MEAN ALTITUDE VS. TIME (CAMERA #1)

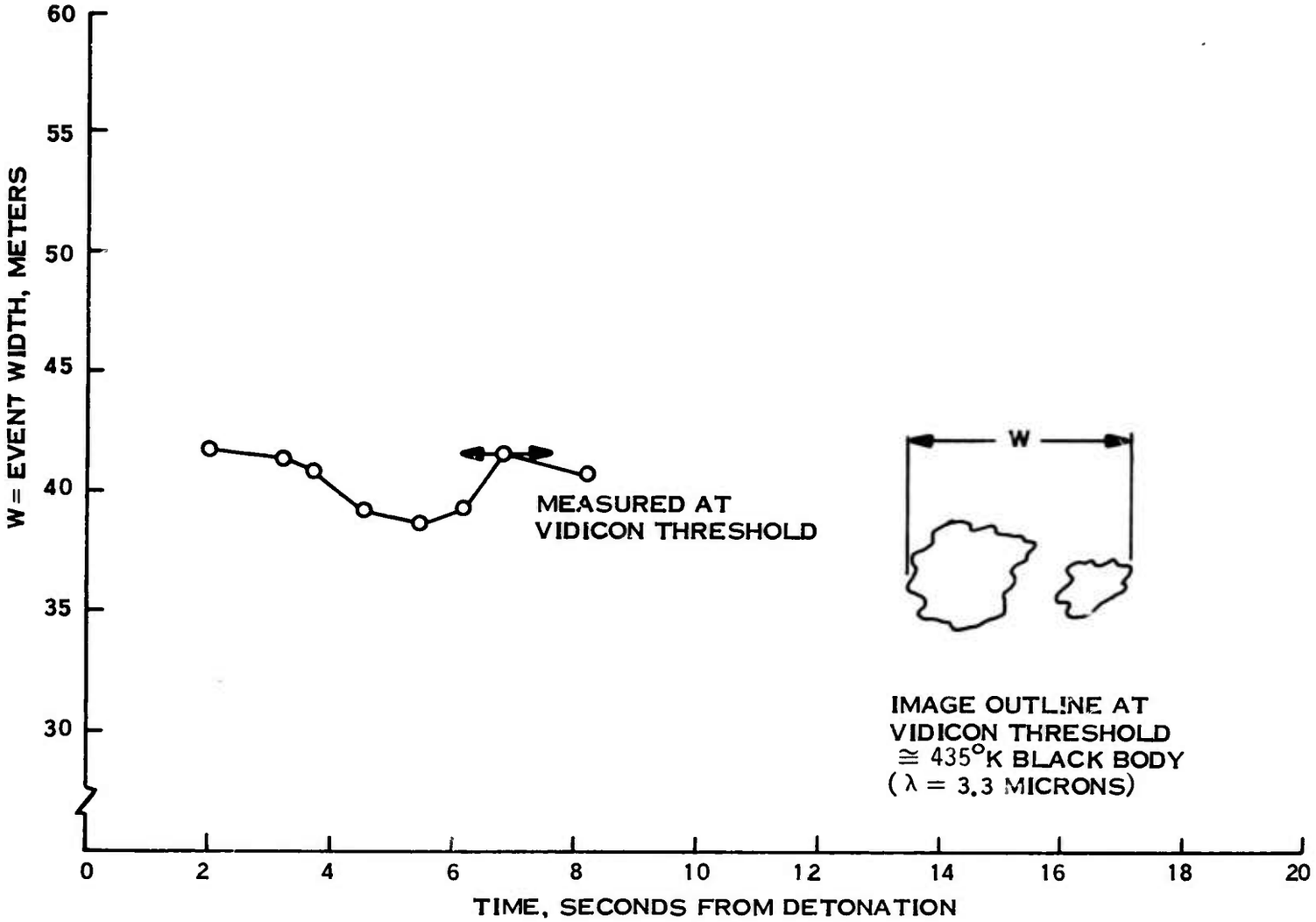

FIGURE 8. IMAGE WIDTH VS. TIME (CAMERA #1)

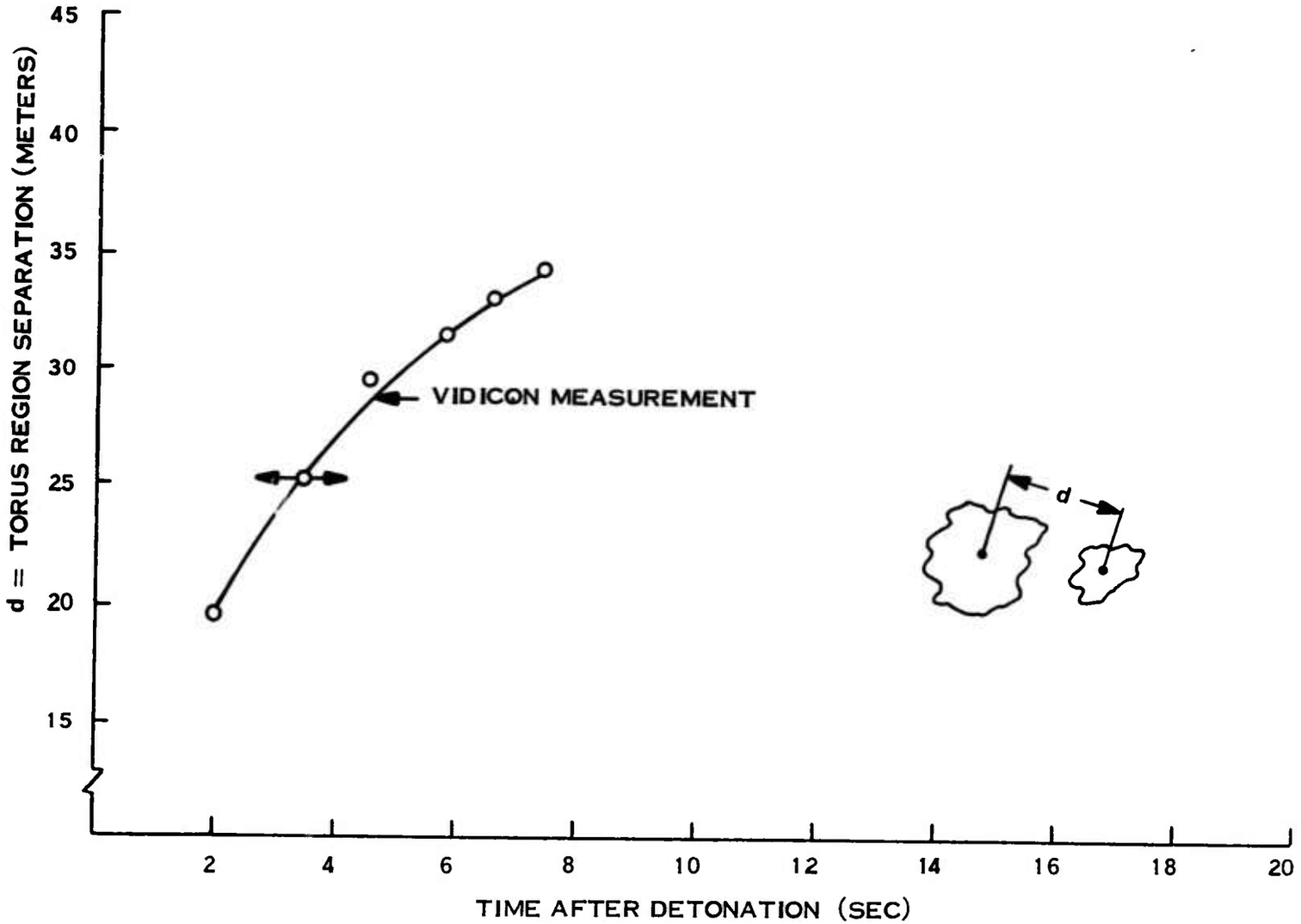

FIGURE 9. TORUS REGION SEPARATION VS. TIME (CAMERA #1)

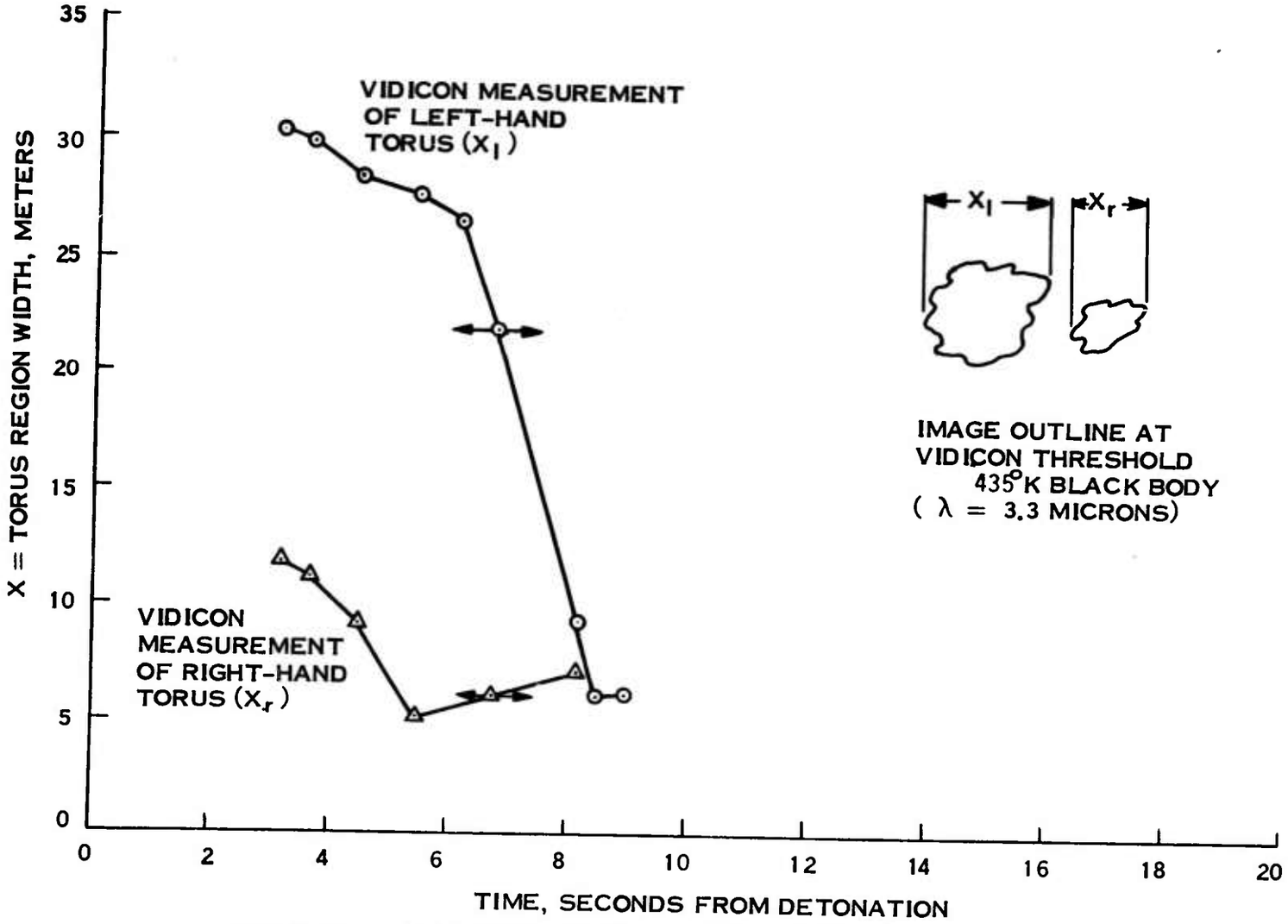

FIGURE 10. TORUS REGION WIDTH VS. TIME (CAMERA #1)

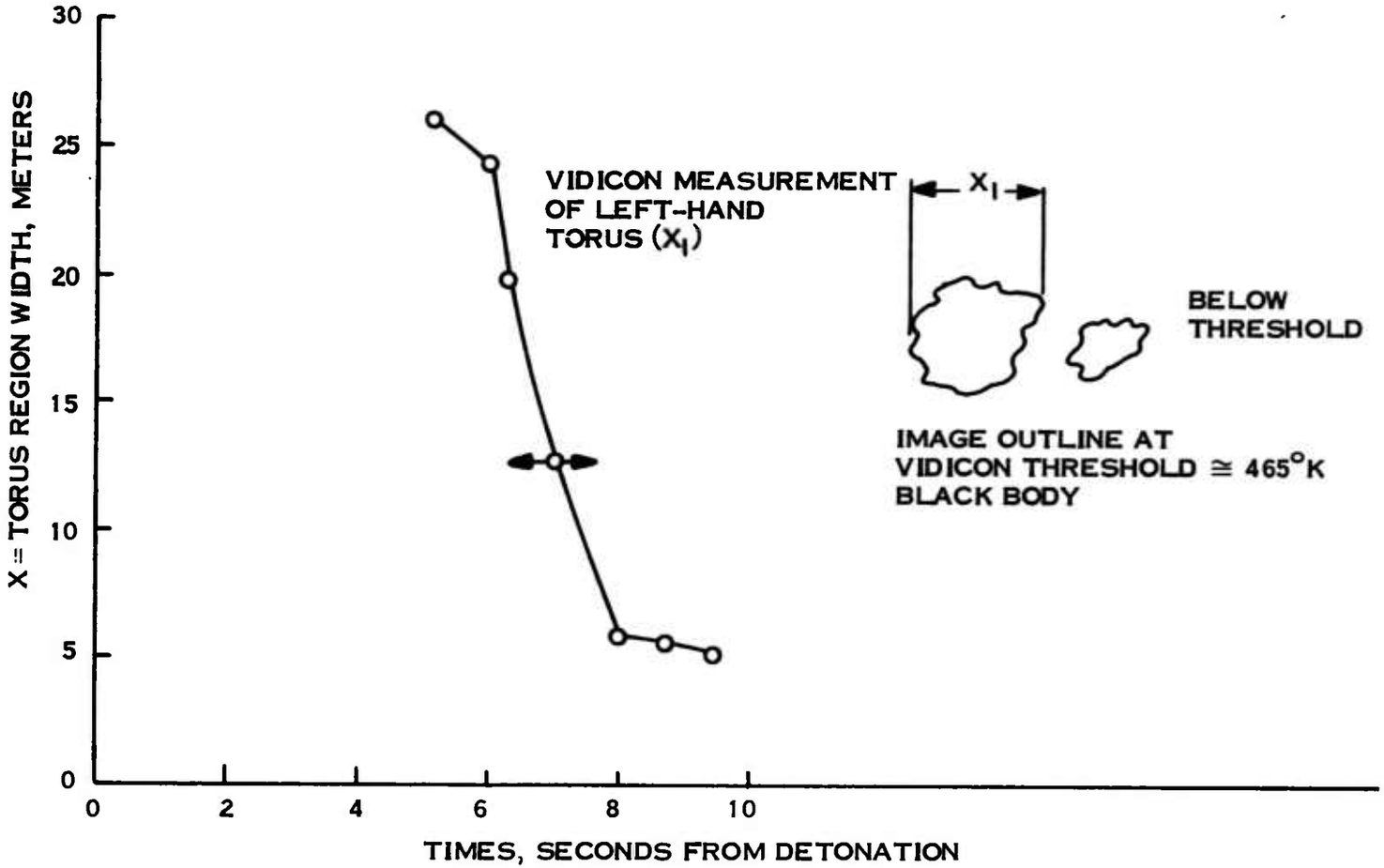

FIGURE 11. TORUS REGION WIDTH VS. TIME (CAMERA #2)

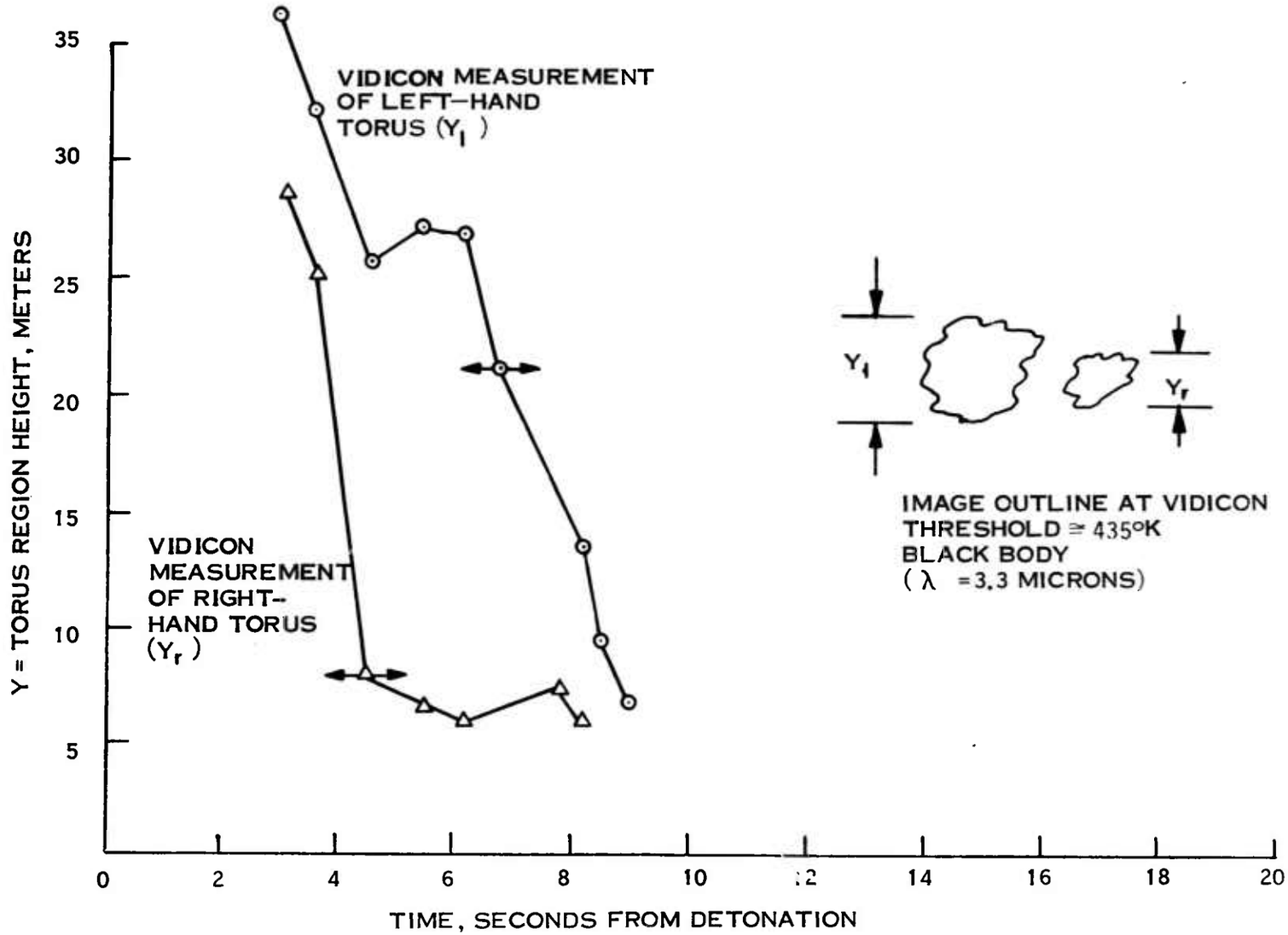

FIGURE 12. TORUS REGION HEIGHT VS. TIME (CAMERA #1)

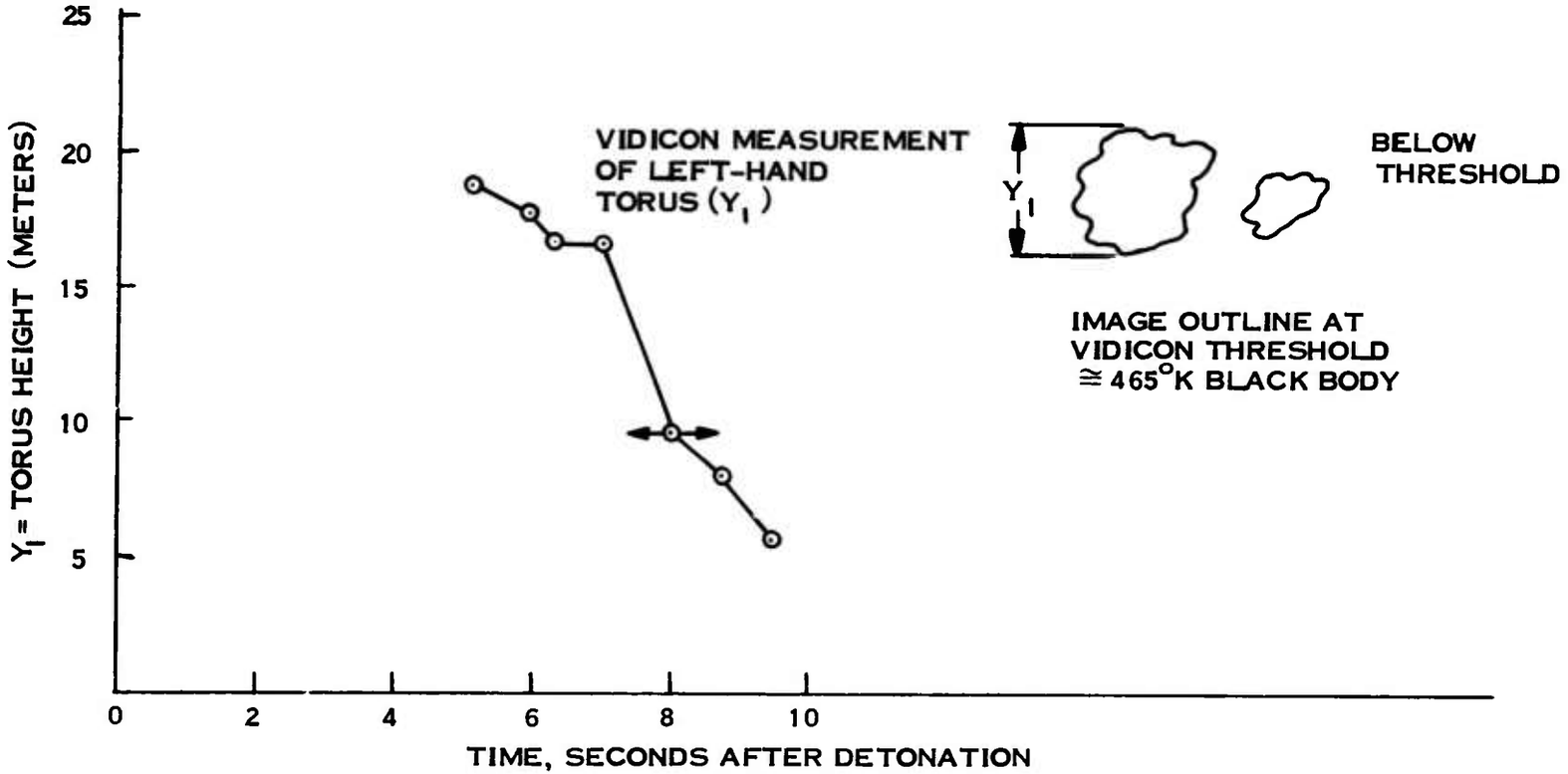

FIGURE 13. TORUS REGION HEIGHT VS. TIME (CAMERA #2)

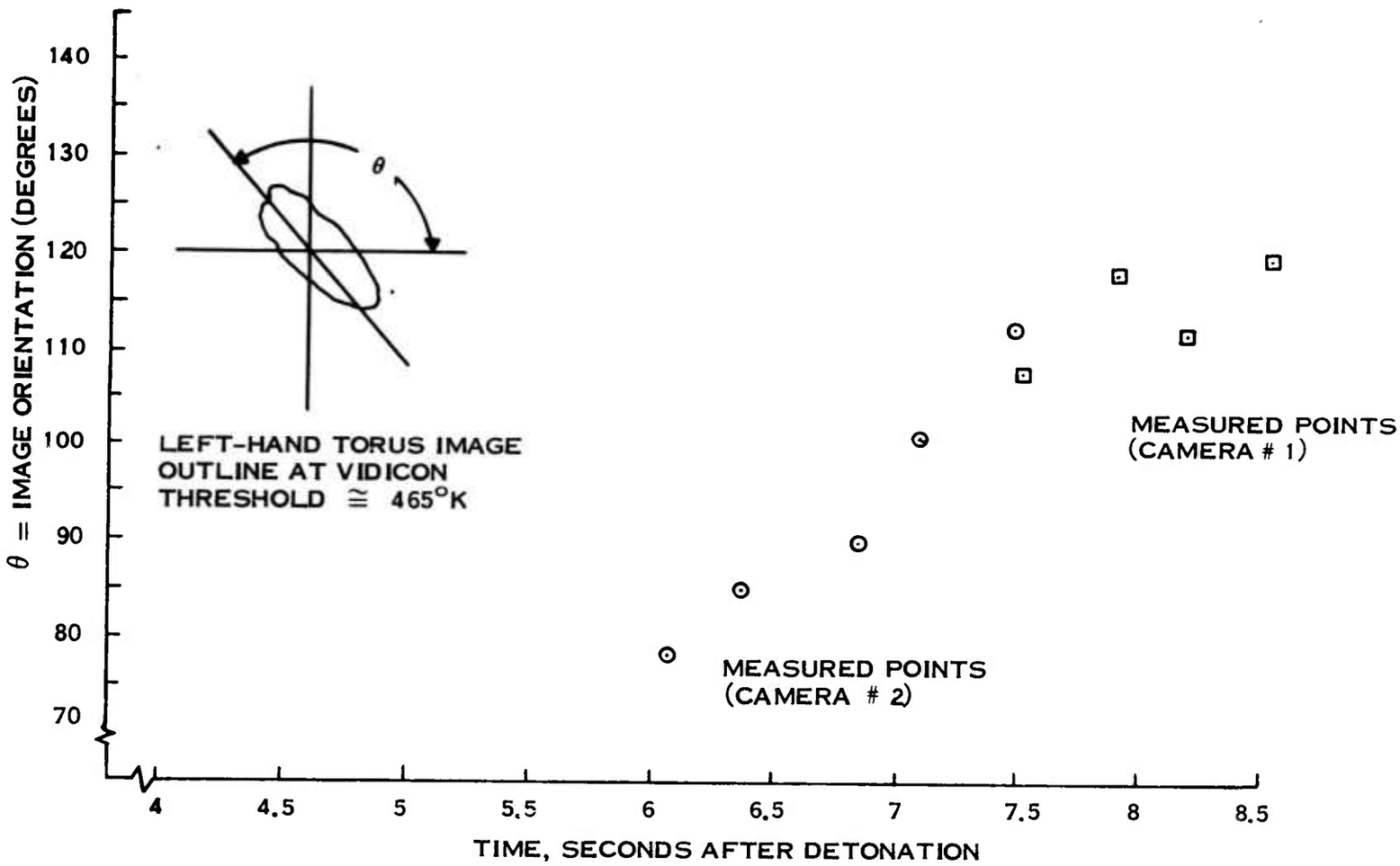

FIGURE 14. TORUS ORIENTATION VS. TIME

seconds, show the continued rise of the roughly spherical cloud (see Figure 7). During this period, the radiant intensity of the cloud was rapidly falling, and shortly after the T+1.6 second frame, it fell below the threshold of the vidicon.

At this time, the aperture stop was removed with the results shown in Part 2 of Figure 6. The frame at T + 2.8 seconds and the next frame are interesting in that they show the cloud while the aperture stop was being removed. The dynamic range distribution in Figure 3, indicates that for the Belvoir camera there is an interval in which the scene radiant intensity is below threshold for the stopped vidicon, but above the saturation limit for the unstopped vidicon. The aperture stop was removed manually and therefore required a finite time for complete removal. These two data frames were obtained when the aperture stop was only partially removed and the cloud radiant intensity fell within the dynamic range of the partially stopped vidicon. Cloud flattening and the beginning of torus formation are clearly shown. When the aperture stop is completely removed at T + 3.1 seconds, saturation obscures the details of the central cloud structure.

The next series of data frames, Part 3 of Figure 6 shows further flattening of the cloud and much clearer definition of the torus. By T + 5.0 seconds, the torus is well defined with a very conspicuous size and intensity unbalance between the right and left sides. Actually, the early stages of this imbalance can be seen in the T + 2.8 second frame. These same features are also illustrated by Figures 9-13 which show torus region separation as a function of time and the conspicuous unbalance between the right and left sides.

The final series of data frames, Part 4 of Figure 6 shows the fade-out of the fully developed torus. The frames at T + 7.5 and T + 8.5 seconds show not only the fully developed torus, but also the cross-section of the much brighter left side. At T + 9.5 seconds, the torus simultaneously rises out of the vidicon field-of-view and falls below the instrument sensitivity threshold.

IV. AUTOMATIC IMAGE PROCESSING OF ABSOLUTE SOURCE RADIANCE

IV.1 Introduction

Processing of images for presentation as maps of absolute source radiance is a laborious task. Further, in the case of infrared vidicon images, the procedure is complicated by a non-linear tube response across the vidicon field. This requires application of a point by point correction to obtain meaningful results. For these reasons, the data taken by the Belvoir camera on the 13 December 1973 balloon explosion have been reduced to absolute source radiance using the GE Image 100, an interactive, automatic image processor. This section describes the operation of the GE Image 100, the data reduction procedure and presents results for absolute source radiance in the form of iso-intensity contours with cross plots of intensity vs. position.

IV.2 Description of Image 100

The General Electric Company has designed, developed, and manufactured a multispectral image analysis system designated "Image 100" (Interactive Multispectral Analysis System) which provides rapid computerized processing of the data from imaging sensors. This tool is heavily used for classification and thematic processing of multi-color imagery from the ERTS (Earth Resource Technology Satellite) multispectral scanner (MSS). In this application, single frames of four colors (spectral channels) are subjected to thematic analysis to establish such information as soil typing and crop yield estimation.

In the present application, data reduction requirements differ from the usual ERTS case in that:

1. Frame-to-frame data reduction is necessary to establish radiometric histories.
2. Point by point shading corrections are required to remove the non-linear response of the vidicon across the field-of-view.
3. The required output is a map of the radiation source which must be related to an absolute radiometric calibration.

Fortunately, the processing capabilities of the Image 100 can be adopted to the present requirements.

Specifically, the Image 100 has the ability to:

1. Reduce data on a frame-by-frame basis using film transparencies as input.
2. Divide a data frame by a reference frame on a point by point basis which allows correction for the non-uniform response within the vidicon field.
3. Classify and display all picture elements the intensity of which falls between operator specified limits, i.e., display iso-intensity contours.

In addition, a densitometer processor is available to plot intensity vs. vertical distance for any selected horizontal position.

Operationally, the Image 100 uses film transparencies as input. These are placed on a light table which is viewed by a TV camera. The video output is passed through an A/D converter and is then stored on a rapid access, large capacity magnetic disc. These data are then available for further processing using a dedicated digital computer and associated display hardware.

IV.3 Data Reduction Procedure

Reduction of the infrared vidicon measurements to absolute source radiance was performed on a frame-by-frame basis. The video data tapes were examined using an Ampex VR 7000 recorder in the stop frame mode. Selected frames were then photographed to produce film transparencies for input to the Image 100. During the photographic processing, care was taken to assure an exposure such that the film was in the linear region of the H and D curve while developing was performed using a unity γ. All frames, background (pre and post-mission), calibration and data were processed with identical conditions.

The cautions cited above in preparation of the film transparencies were not sufficient to assure constant film density between frames. The problem was traced to a background brightness variation from frame to frame. This, in turn,, was caused by poor frequency regulation in the field power source used for the infrared vidicon system. To circumvent this difficulty, each calibration and data frame was matched to a background frame having equal density characteristics in regions where no data or calibration signal was present. This background level represents an effectively constant focal plane background radiance across the field-of-view with the optics assembly as the dominant

contributor. (The vidicon raster position and size were set to avoid severe vignetting regions at the retina edge.)

A background frame was next selected and defined as a standard. This was placed on the light table of the Image 100 and the brightness adjusted to give a grey scale reading in the center of the dynamic range of the instrument at a selected standard location. Thus, any other background transparency could be referred to the standard either by adjusting the table brightness to the measured standard grey scale at the standard location or by a simple multiplicative scaling using the measured grey scales at the standard location. In practice, the table brightness adjustment was accurate to $\pm$ 10%. The remaining normalization was performed by scaling.

Data and calibration frames were keyed to their matched reference background frames by the same procedure. In this case, a second reference location which was free from data or calibration signal was used to adjust the grey scale to the standard. This procedure is based on the constant focal plane radiance across the field-of-view which originates at the optics assembly of the infrared vidicon. Thus, all frames have been normalized to a standard grey scale, i.e., data or calibration were normalized to matched reference background which in turn was normalized to standard background. Processing of all data and calibration frames was identical and consisted of:

1) Loading the matched background frame onto the magnetic disc of the Image 100.
2) Adjusting the brightness to the standard grey scale.
3) Loading the data frame on a second channel of the magnetic disc.
4) Dividing the data frame by the matched background frame to correct for vidicon response.
5) Performing the iso-intensity contour analysis.
6) Using the densitometer processor to obtain cross plots of intensity vs. vertical distance at selected horizontal locations.

Loading the standard, background reference, data and calibration frames into the Image 100 consisted of placing the transparency on the light table of the instrument. Alignment was provided by fiducial marks on the front face of the TV monitor which was photographed to produce the original transparencies. As a verification, the position of the tube blemish on the Belvoir camera (see

Figure 5) was checked to assure consistency with the field measurement geometry. This procedure produced frame to frame variations which were better than the resolution of the infrared vidicon system ~1/3 meter.

Figure 15 presents densitometer scans of a typical reference background frame. The traces represent the non-linear vidicon response across the field-of-view. Examination of these results indicates that variations as large as a factor of four are present in the uncorrected data. On the other hand, when either data or calibration frames were divided by the matched reference background frame, the densitometer scans were flat in those regions where data was absent. It is thus concluded that the tube response variations were removed by the correction procedure.

The iso-intensity contour analysis was performed in an interactive manner. Upper and lower limits for the intensity were selected such that the upper limit was slightly above peak signal and the lower limit was just above background. This range was then subdivided into seven equal increments. All picture elements having intensities falling between these subdivided limits were then displayed on a color TV monitor using a separate color for each contour. The results were examined and the limits re-adjusted to obtain the best iso-intensity contour analysis. In practice, seven individual contours could not be identified because of overlap caused by noise. Consequently, only those which were resolvable were recorded for presentation in the report.

Densitometer traces were prepared by subdividing the data frame into eleven equally spaced horizontal increments. Scans (plots of standard grey scale vs. vertical distance) were then recorded at those locations where data were present. The results were hand smoothed and the grey scale was converted to absolute intensity using the calibration data discussed in the next section.

IV.4 Calibration

The Belvoir camera was calibrated following the 13 December 1973 test by observing a 12 inch x 12 inch black body source located approximately 50 feet from the camera. The calibration data were reduced and plotted by the method defined in Section II.3 to obtain the calibration curve shown in Figure 4. However, when using the Image 100 for data reduction, the following interpretation is applied to the calibration results.

The standard gray scale, G_{STD}, measured by the Image 100 corresponds to

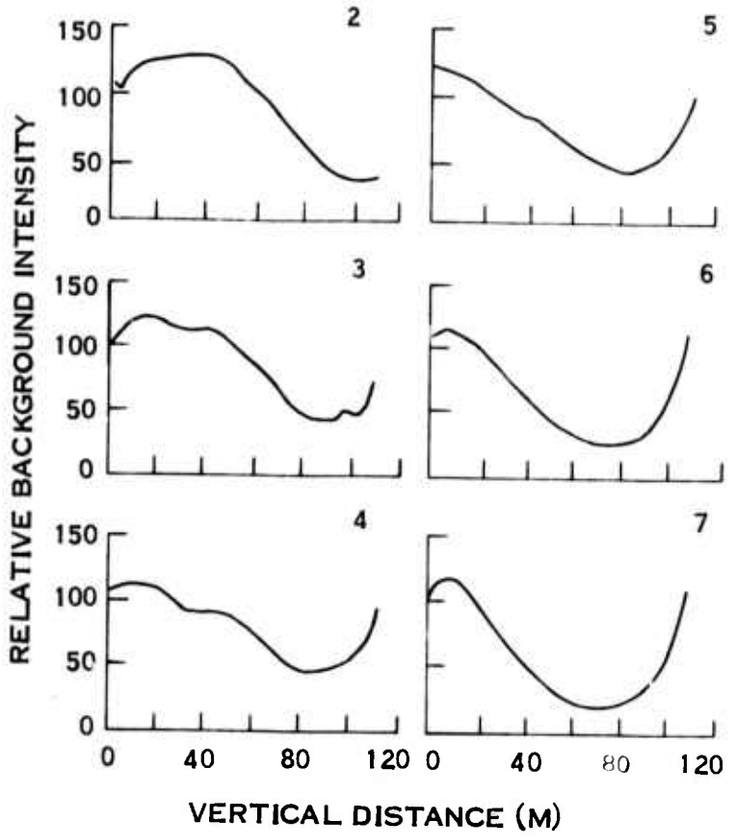

FIGURE 15. DENSITOMETER SCANS OF REFERENCE BACKGROUND FRAME

the sum of the target and background vidicon focal plane irradiance. The retina background irradiance is dominated by that from the rear of the spectral filter and vidicon faceplate. The target irradiance is determined by a transfer function of the type given by Equation (1). Because the vidicon system is dominated by electronic noise, and because this noise is constant for a given camera setting, S/N is proportional to the standard gray scale derived from the Image 100 measurements, i.e.,

$$G_{STD} = C_1 \quad S/N$$

where:

C_1 = calibration constant for Image 100 processing

S/N = signal-to-noise ratio

Thus:

$$G_{STD} = C_1 C_2 \ (H_{CAL} + H_{BACK}) \qquad (2)$$

where:

C_2 = a constant relating S/N to irradiance

H_{CAL} = the retina irradiance from the calibration source

H_{BACK} = the retina background irradiance

Figure 16 is a plot of G_{STD} vs. H_{CAL}. The slope gives C_1C_2 while the ratio of the intercept to slope gives $H_{BACK} = 1.943 \times 10^{-4}$ watt/cm^2. This agrees with the background obtained when reducing subsequent data, as will be shown later. Figure 17 shows the data plotted in log-log form with H_{BACK} removed. The results verify the linearity of the data processing. In addition, the unity-gamma characteristic of the vidicon sensor and film developing is demonstrated. It is thus concluded that the assumptions used in data reduction are indeed valid.

IV.5 Results

The calibration curve shown in Figure 16 was used to reduce the standard gray scale measurements of the iso-intensity contour limits and of the densitometer scans to absolute source radiance. Referring to Equation (2), the standard gray scale measurements contain a contribution from the retina background irradiance. This was removed by subtraction on a frame-by-frame basis. All densitomter traces recorded for a given frame were examined and the

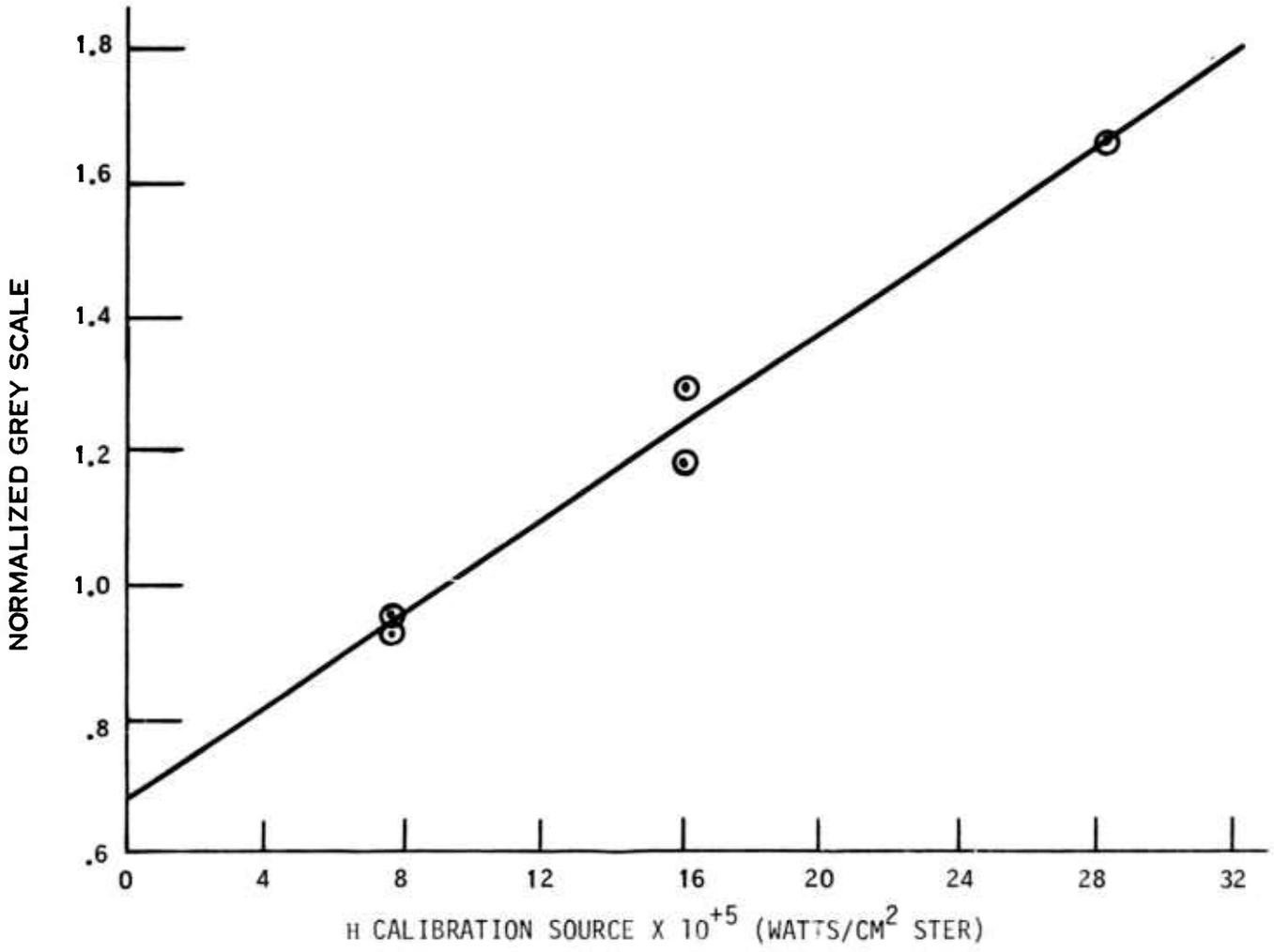

FIGURE 16. CALIBRATION CURVE FOR THE BELVOIR CAMERA DATA AS PROCESSED ON THE IMAGE 100.

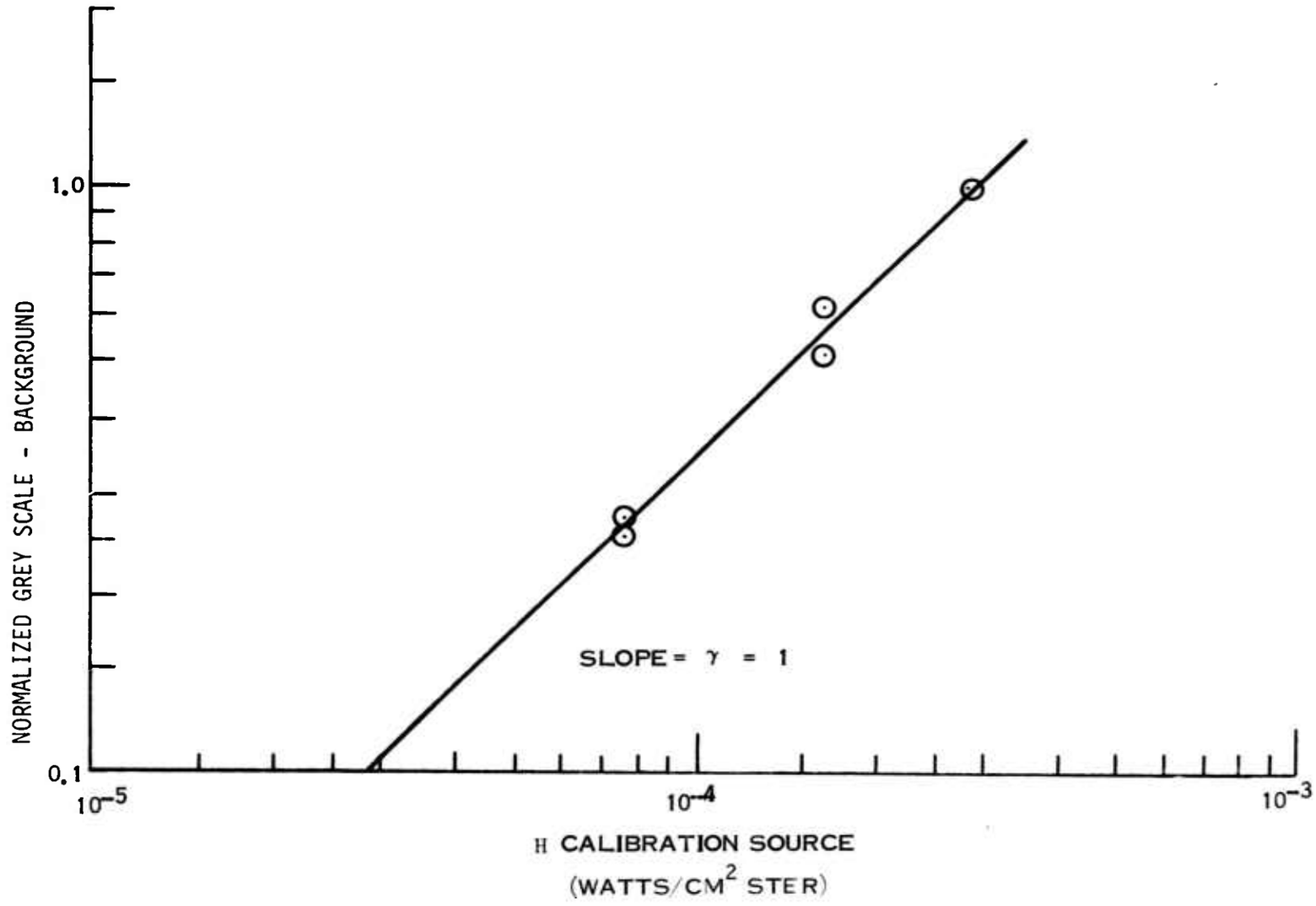

FIGURE 17. CALIBRATION CURVE FOR THE BELVOIR CAMERA DATA WITH BACKGROUND REMOVED ILLUSTRATING UNITY γ OF THE REDUCTION PROCESS.

background level determined at the edge of the image of the balloon debris. These values were then averaged to define the retina background irradiance for the entire frame. This was then removed from the iso-intensity contour limits and also served as the zero for the densitometer traces.

Examination of the retina background irradiances shown in Table I provides an estimate of the precision of the measurements. It is first noted that the average retina background irradiance determined from the data transparencies agrees well with that derived from the intercept of the calibration curve (1.876×10^{-4} compared to 1.943×10^{-4} watts/cm^2). Further, the variation within any given frame is $\pm$ 10%. This same confidence interval is also derived from the variance of all frames using the standard t-distribution at the 95% level. Even though the radiometric precision of the measurements is excellent, the reader is cautioned that the retina background irradiance is large and that for the lowest levels reported the absolute source radiance can be in error by as much as a factor of two.

The retina irradiance produced by the debris of the balloon explosion was next converted to absolute source radiance by evaluating the convolution integral of the radiometric transfer function. AFCRL measured spectra of the events from a field location adjacent to that of the vidicon camera system. These data (Reference 4) show that the convolution integral can be approximated by a simple product, i.e.,

$$\int \Delta N_{\lambda_{(c)}} R^1(\lambda)\, T_a(\lambda)\, T_o^1(\lambda)\, T_f^1(\lambda)\, d\lambda$$

$$\sim \Delta N_{\lambda_{(c)}}\, T_a(\lambda)\, C_3$$

where:

$$C_3 = 0.088\mu$$

$$T_a(\lambda) = 0.78$$

The atmospheric transmission was taken from AFCRL computation using 4 cm^{-1} resolution and the conditions which prevailed at the test site (Reference 4).

Results for the iso-intensity contours and densitometer scans are presented in Figures 18 to 28. Each iso-intensity contour is labelled numerically for reference to the legend on the figure. Lower limits are marked with a < symbol which implies that all intensities outside the contour are less than the cited value. Upper limits are indicated by a > symbol which means

TABLE I

RETINA BACKGROUND IRRADIANCE

(WATTS/CM^2 X 10^4)

TIME (SECONDS)	HORIZONTAL POSITION (RELATIVE UNITS) 1	2	3	4	5	6	7	8	9	10	11	AVERAGE
0.083	1.96	1.96	1.96	1.96	1.96							1.96
0.183	1.93	1.93	1.93	1.93	1.93	1.93	1.93					1.93
0.35	1.55	1.63	1.55	1.55	1.63	1.63						1.59
0.93	1.37	1.37	1.42	1.42	1.42	1.42	1.42					1.41
1.05	2.12	2.04	2.12	2.12	2.12	2.12	2.12					2.11
1.47	2.39	2.55	2.55	2.71	2.55	2.55	2.39	2.39				2.51
2.40	1.75	1.75	1.75	1.82								1.77
2.65	1.46	1.46	1.46	1.46	1.46	1.46	1.46	1.46				1.46
3.56	2.01	2.01	2.01	2.01	2.01	1.81	1.61	1.61				1.89
4.50	1.99	1.99	1.99	2.18	1.99	1.99	1.99	1.99	1.79	1.79	1.79	1.95
6.00	2.25	2.25	2.06	1.87	1.86	2.06						2.06
									AVERAGE			1.876
												± 10%

that all regions within the contour are saturated and that the intensity is greater than the cited value. The arrows at the top of the iso-intensity contour map show the horizontal locations of the densitometer scans. Both the arrows and the densitometer scans are numbered for easy reference.

The results of the vidicon measurements have been compared to those from the AFCRL interferometer mentioned above. The latter instrument has a wide field and observes the entire debris cloud. For this reason, the iso-intensity maps were integrated to obtain an equivalent signal. In all cases examined, the total source radiance measured by the two instruments was within 50%, with the vidicon measurements being the lower of the two values. This agreement is considered excellent in view of the differences in calibration and test procedures.

(The reverse of this page is blank)

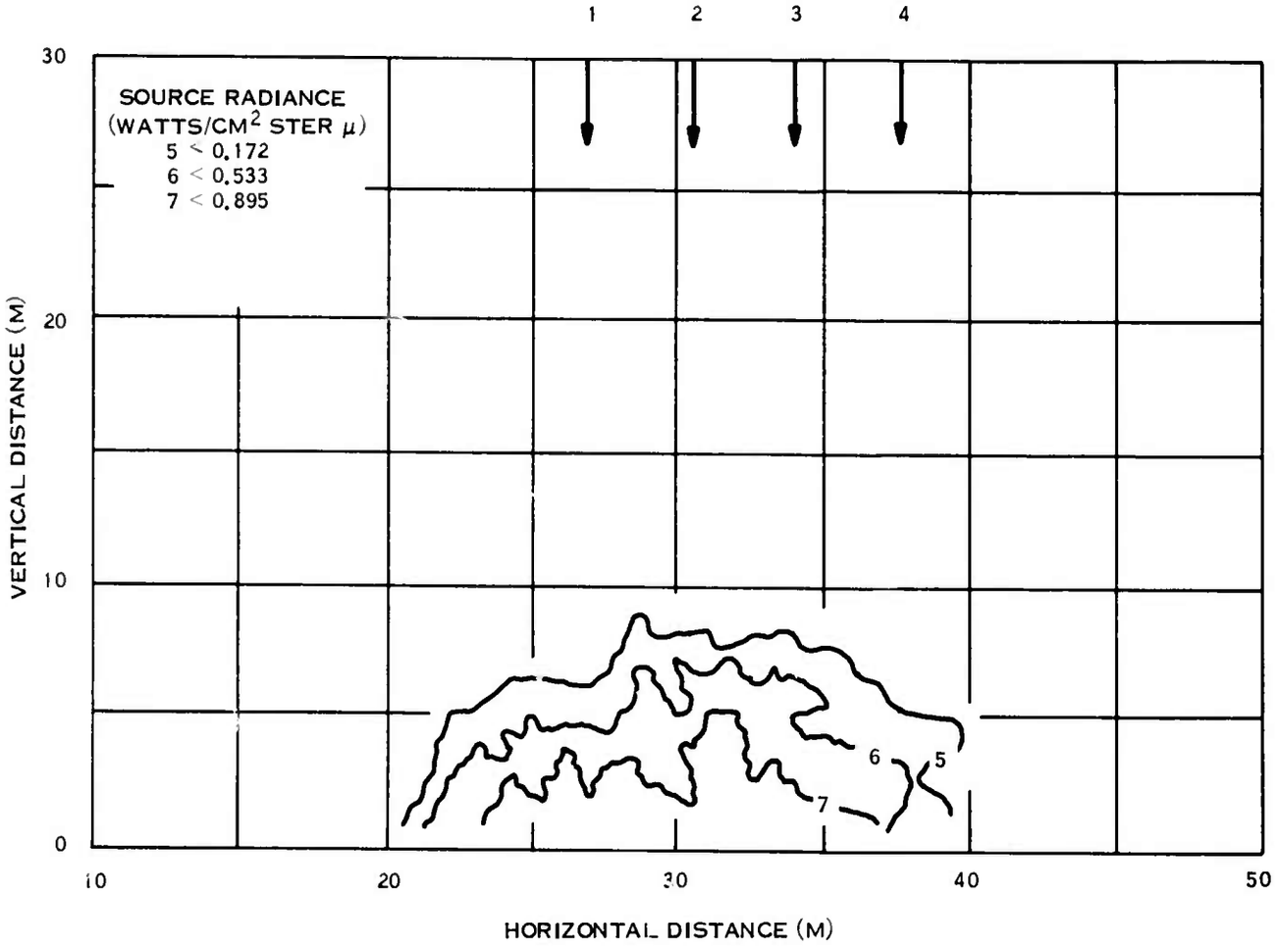

FIGURE 18. SOURCE RADIANCE - ISO-INTENSITY CONTOURS AND VERTICAL DENSITOMETER SCANS. TIME = .083 SECONDS.

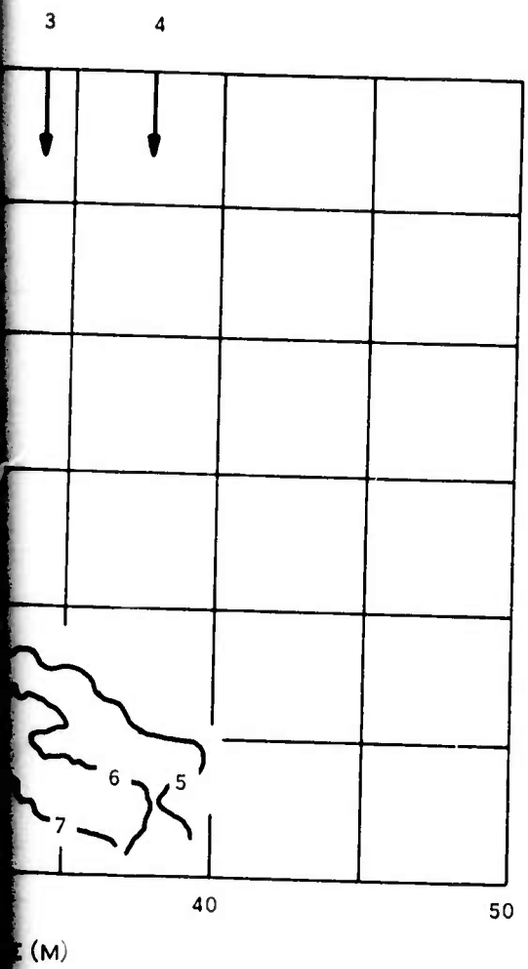

(M)

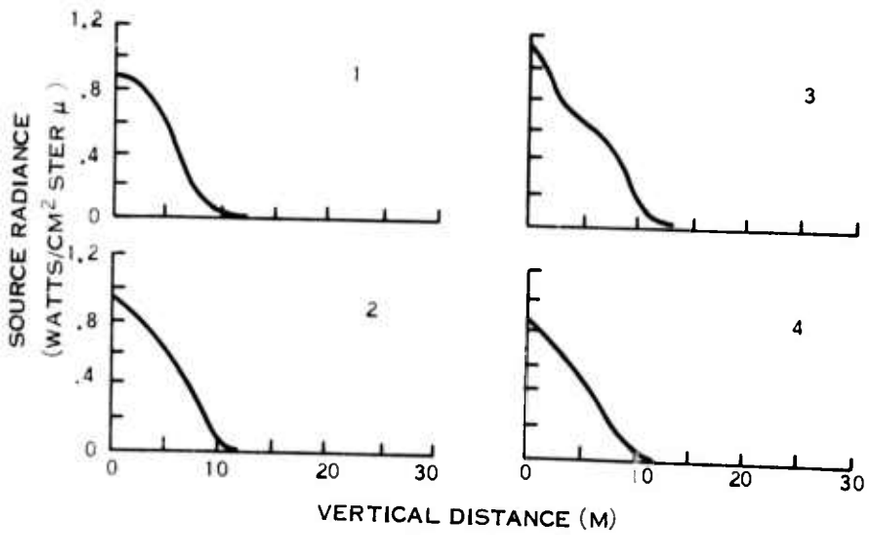

O-INTENSITY
TOMETER
DS.

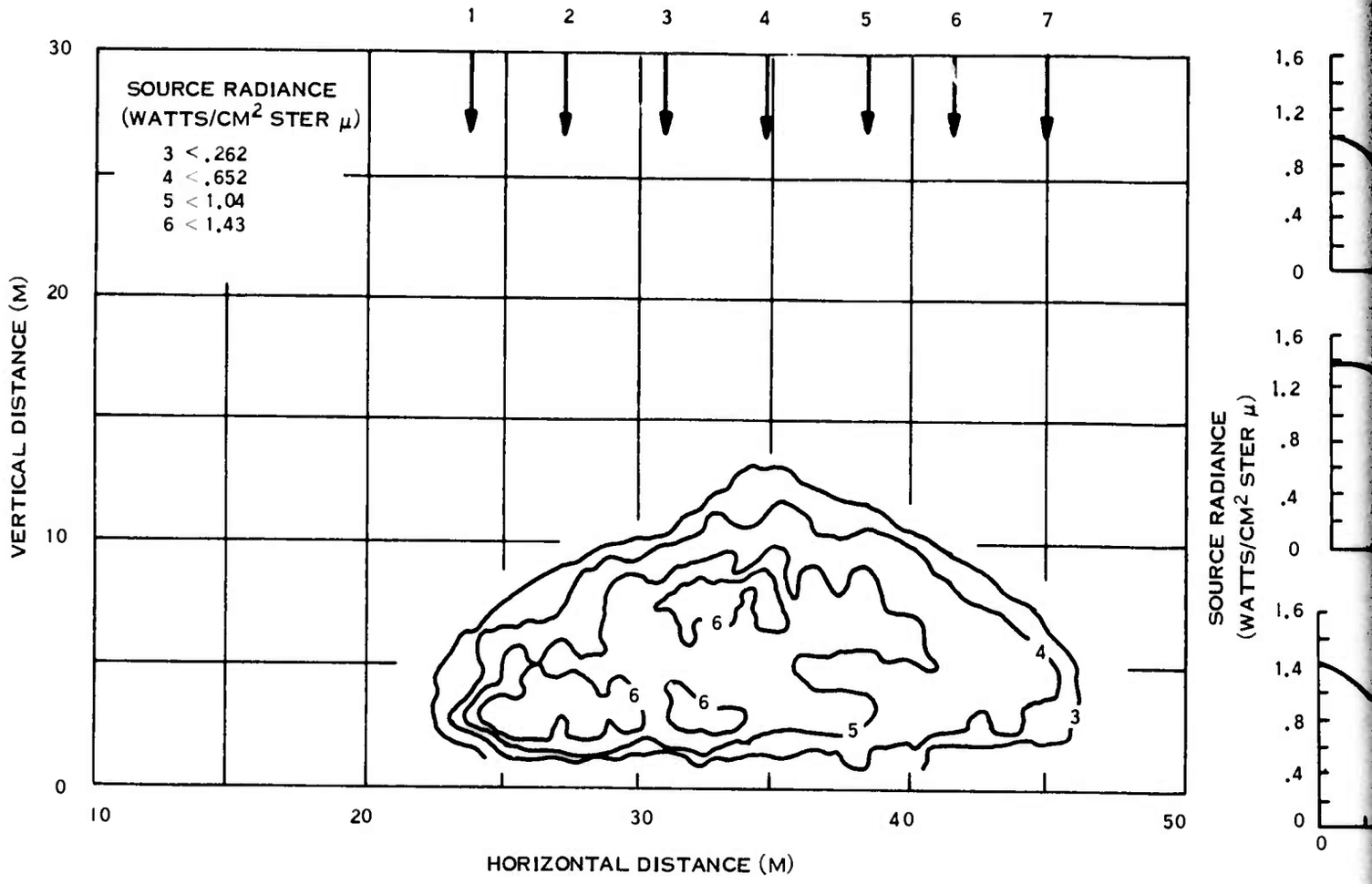

FIGURE 19. SOURCE RADIANCE - ISO-INTENSITY CONTOURS AND VERTICAL DENSITOMETER SCANS. TIME = .183 SECONDS.

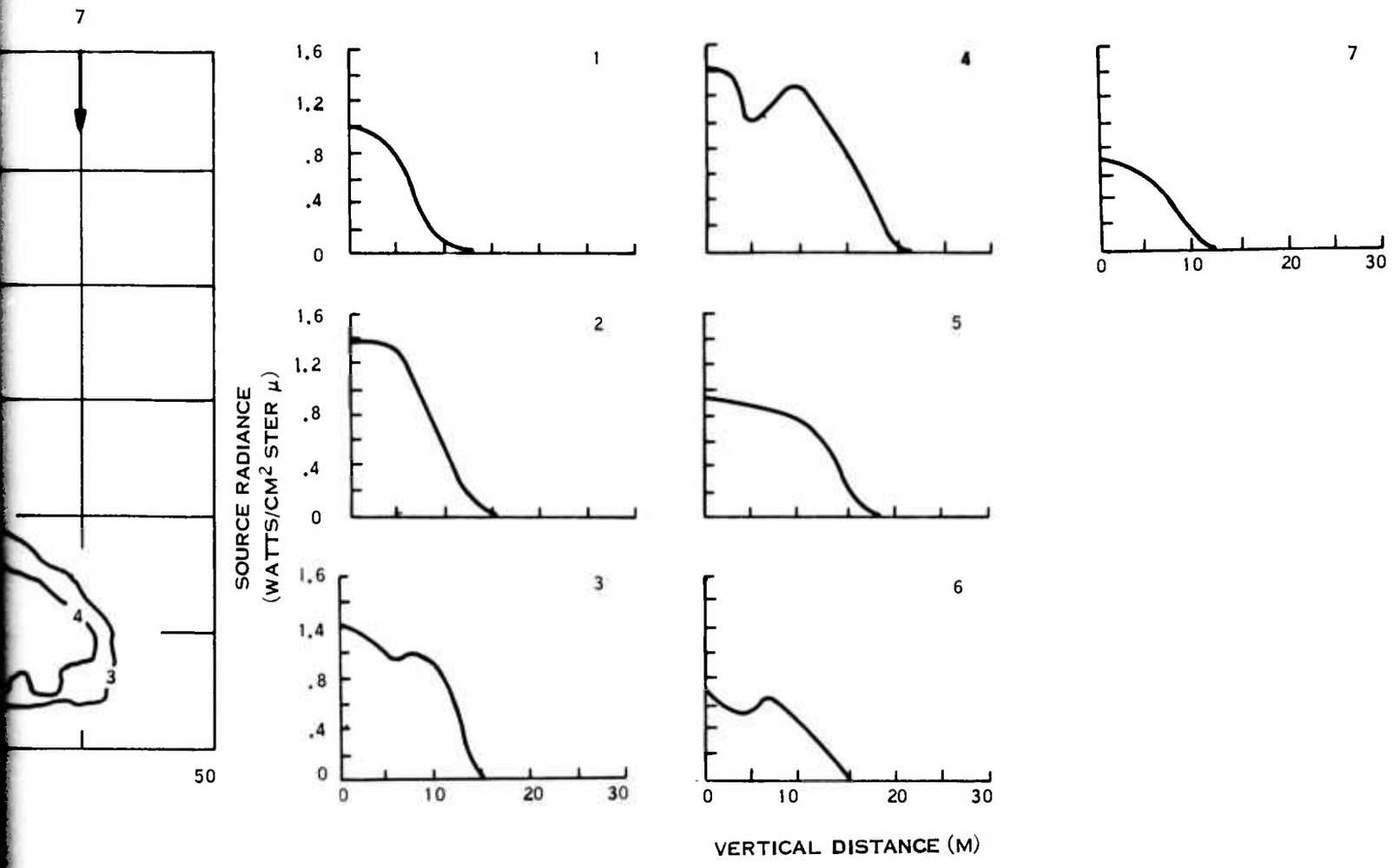
7
4
3
50
1.6
1.2
.8
.4
0
1
2
3
4
5
6
7
1.4
0
10
20
30
SOURCE RADIANCE
(WATTS/CM² STER μ)
VERTICAL DISTANCE (M)

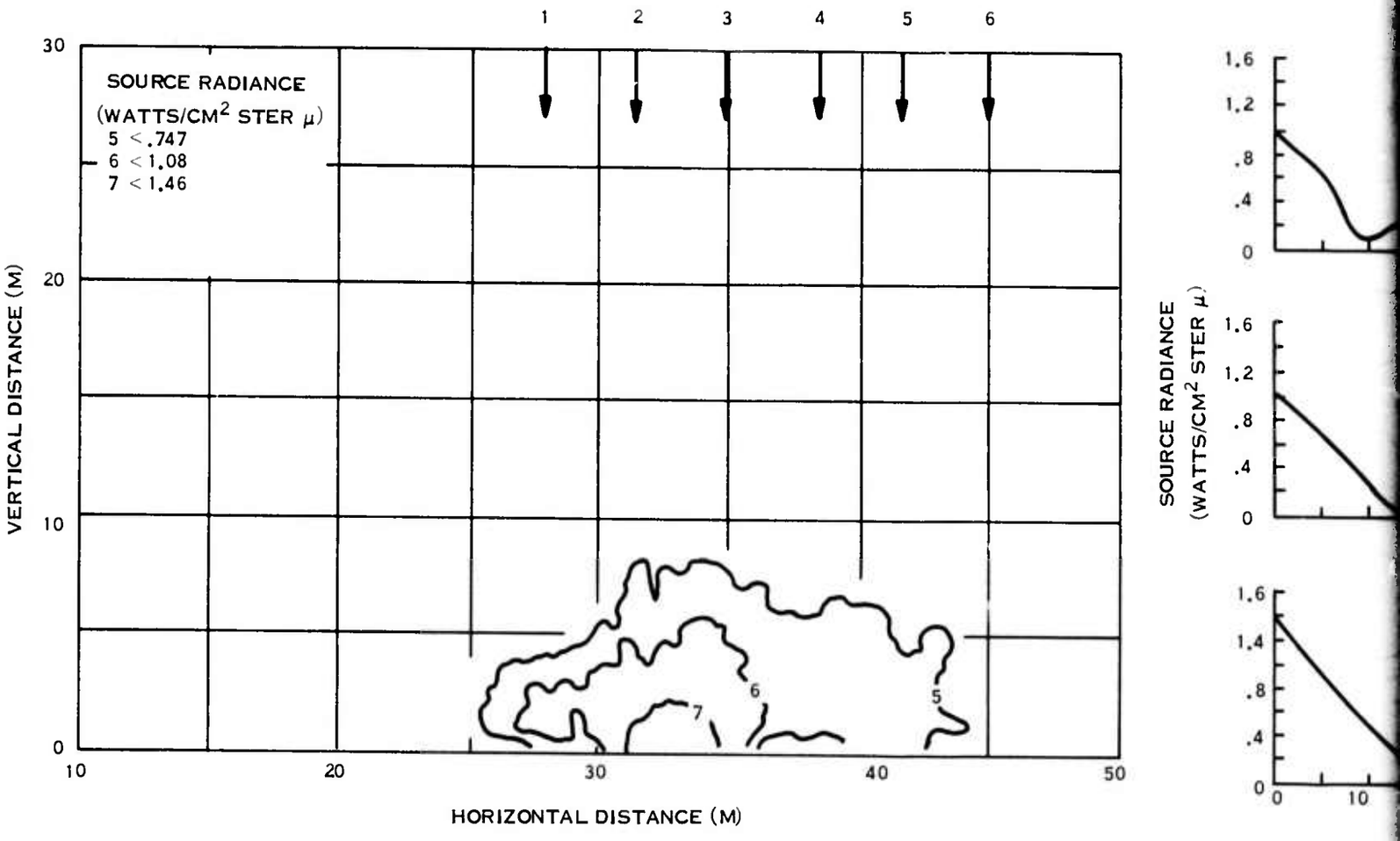

FIGURE 20. SOURCE RADIANCE - ISO-INTENSITY CONTOURS AND VERTICAL DENSITOMETER SCANS. TIME = .35 SECONDS.

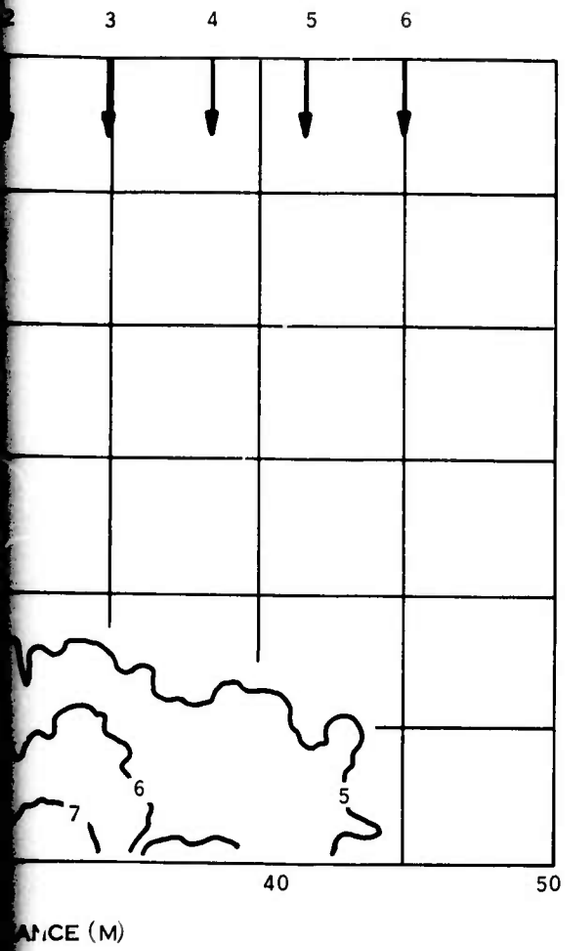

ANCE (M)

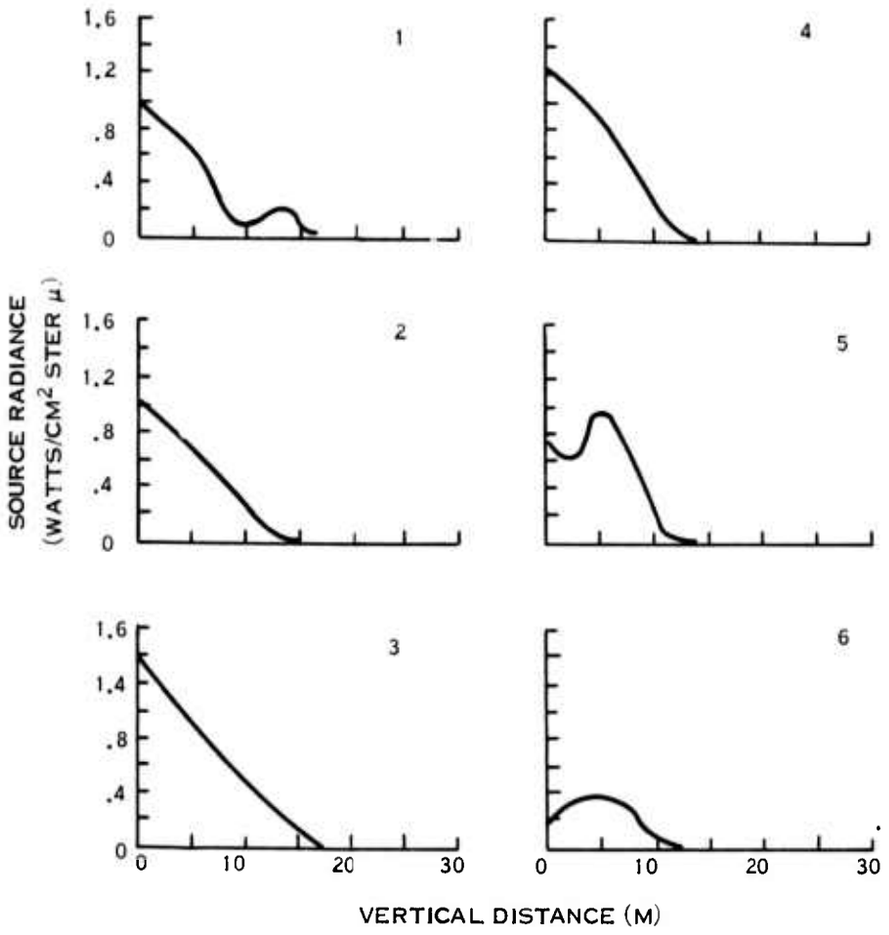

- ISO-INTENSITY
DENSITOMETER
ECONDS.

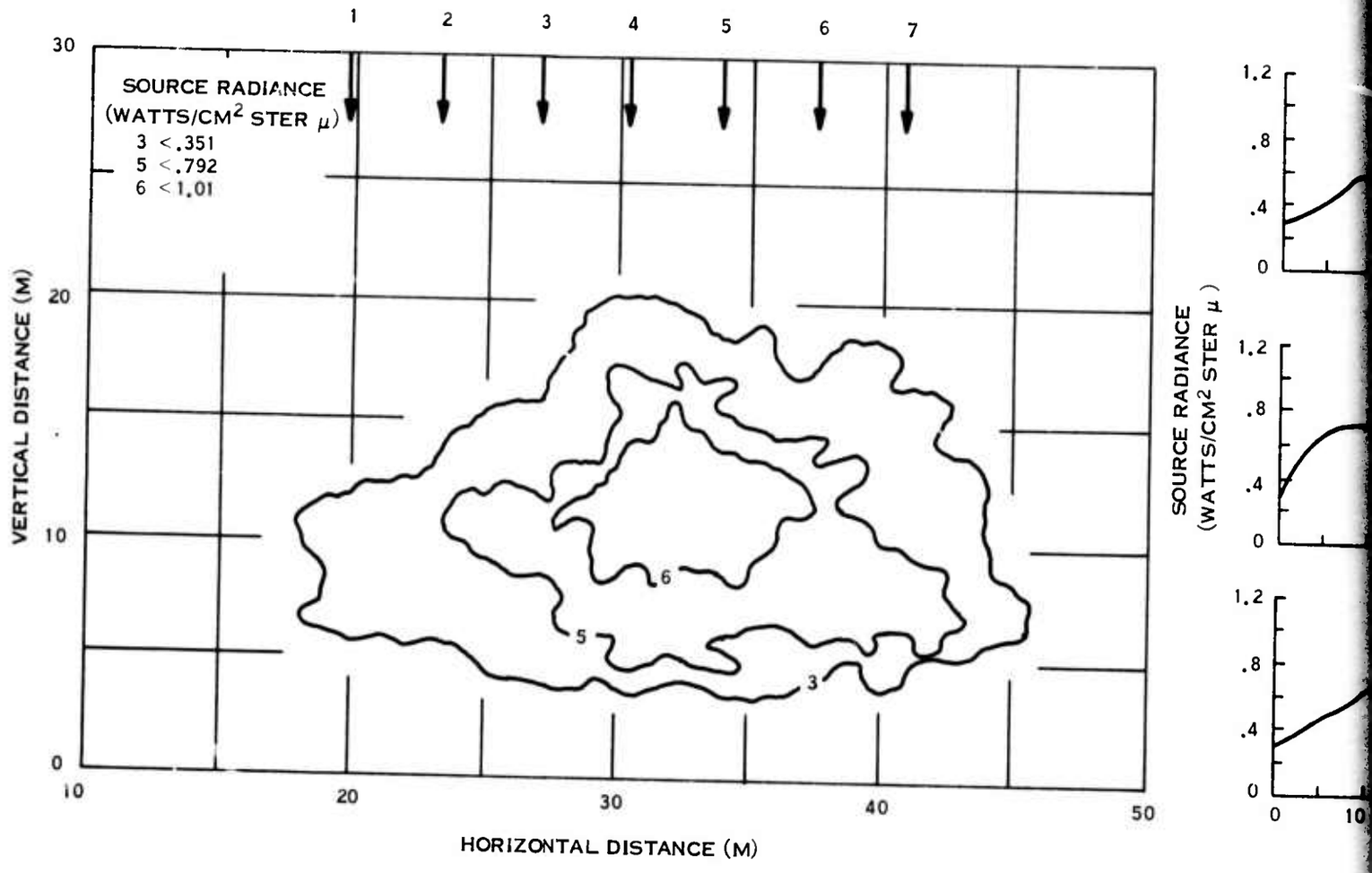

FIGURE 21. SOURCE RADIANCE - ISO-INTENSITY CONTOURS AND VERTICAL DENSITOMETER SCANS. TIME = .93 SECONDS.

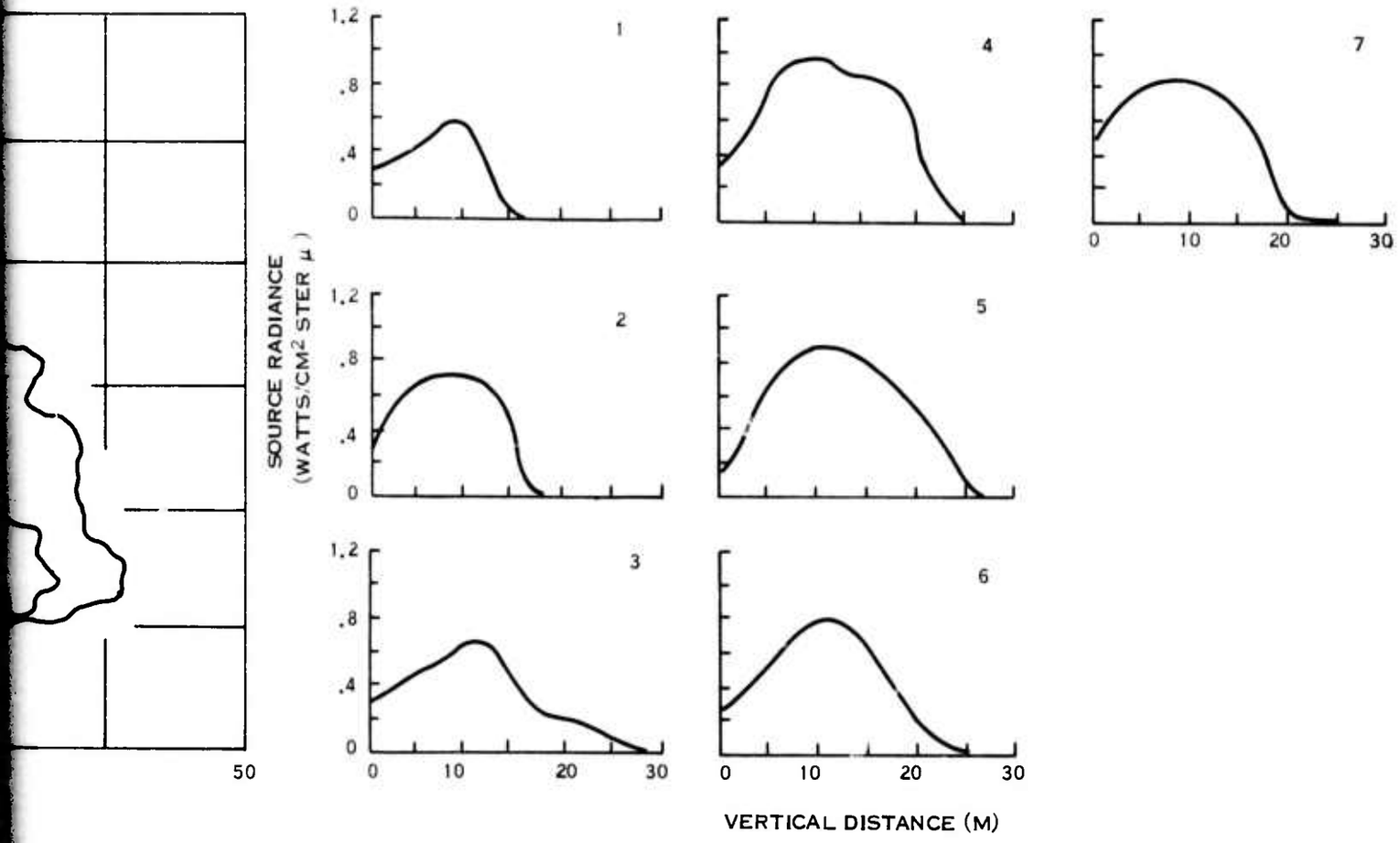
1.2
.8
.4
0
1
2
3
4
5
6
7
0
10
20
30
50
SOURCE RADIANCE
(WATTS/CM² STER μ)
VERTICAL DISTANCE (M)

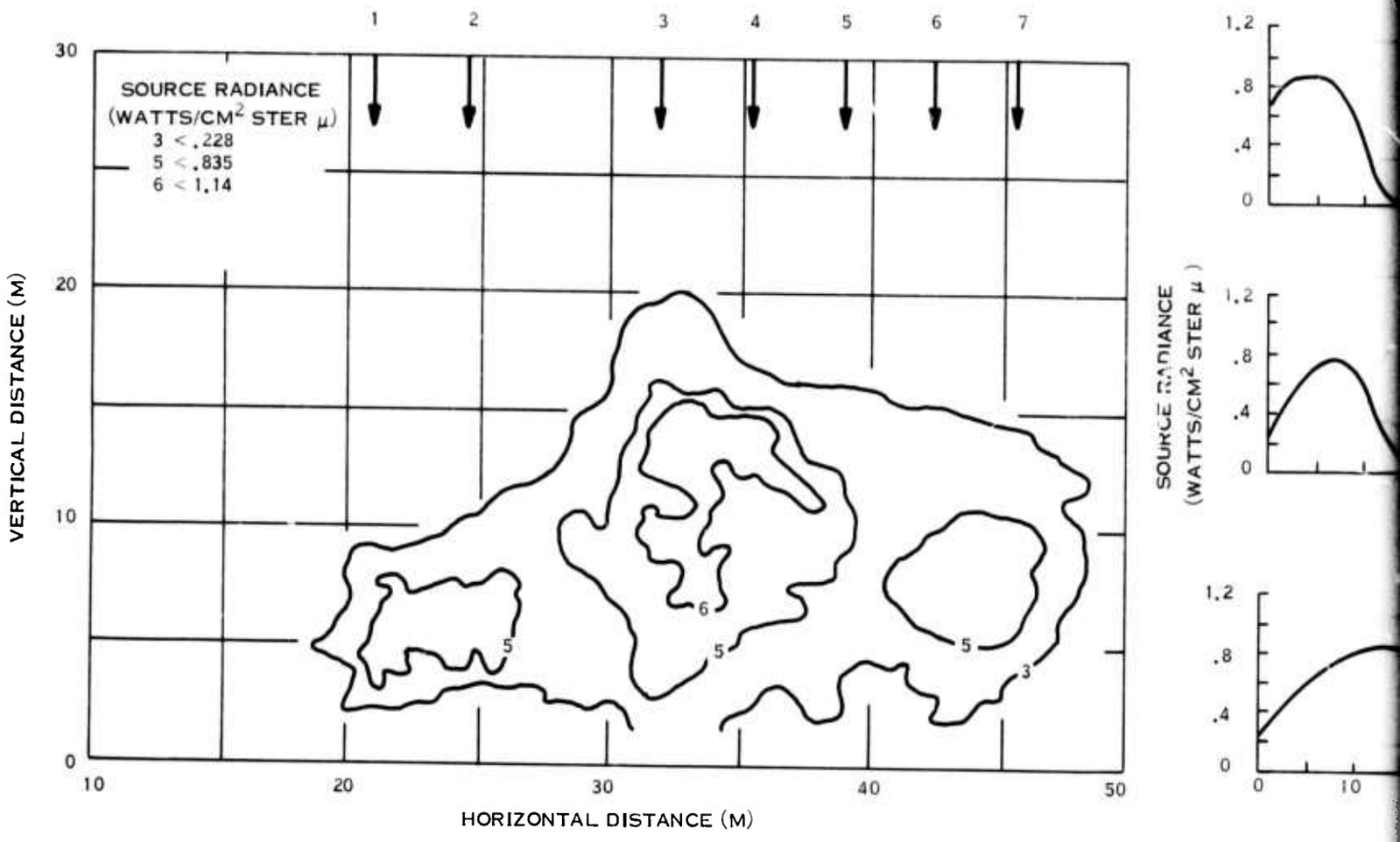

FIGURE 22. SOURCE RADIANCE - ISO-INTENSITY CONTOURS AND VERTICAL DENSITOMETER SCANS. TIME = 1.05 SECONDS.

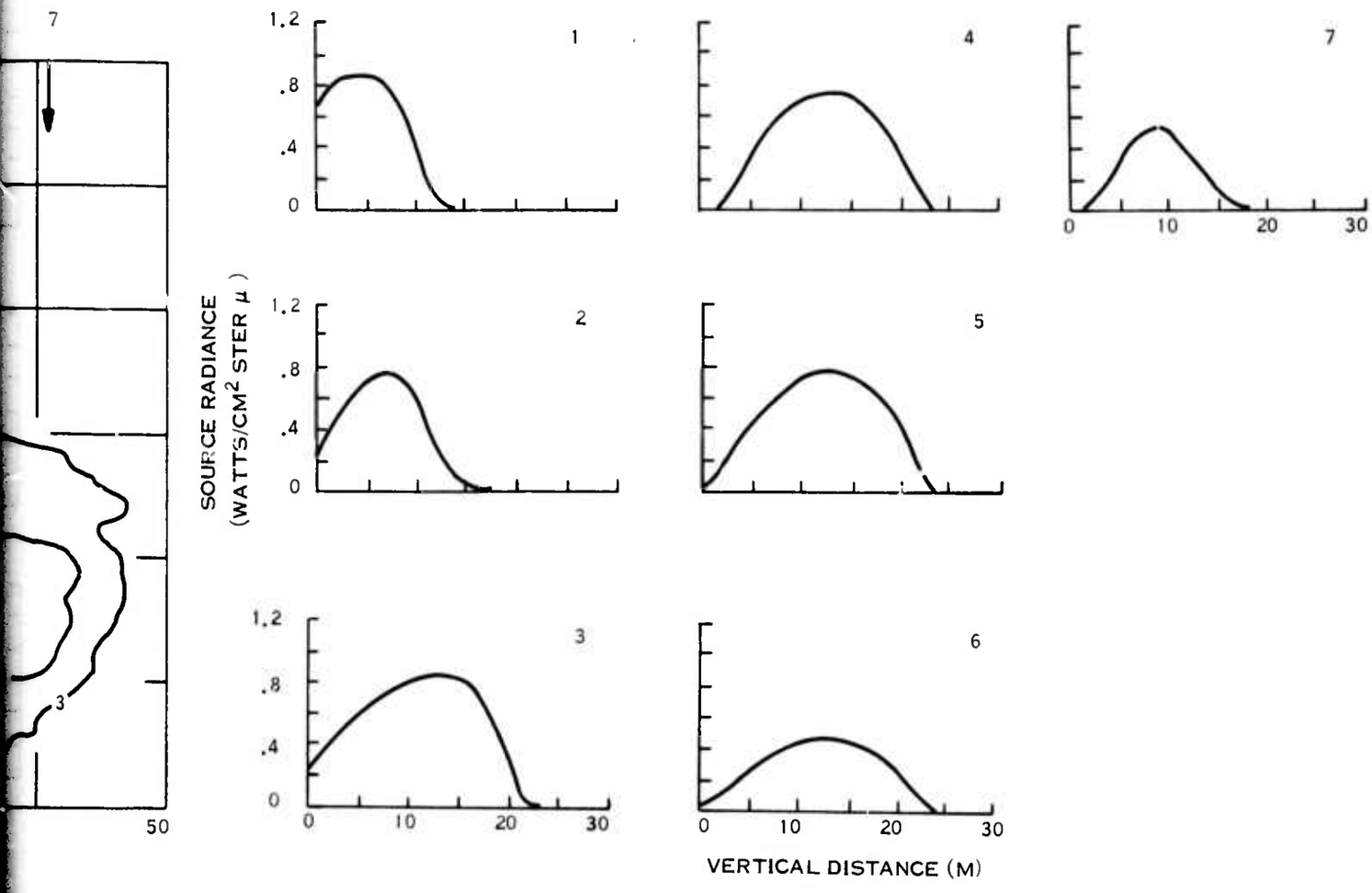
7
3
50
1.2
.8
.4
0
1
2
3
4
5
6
7
0
10
20
30
SOURCE RADIANCE
(WATTS/CM² STER μ)
VERTICAL DISTANCE (M)

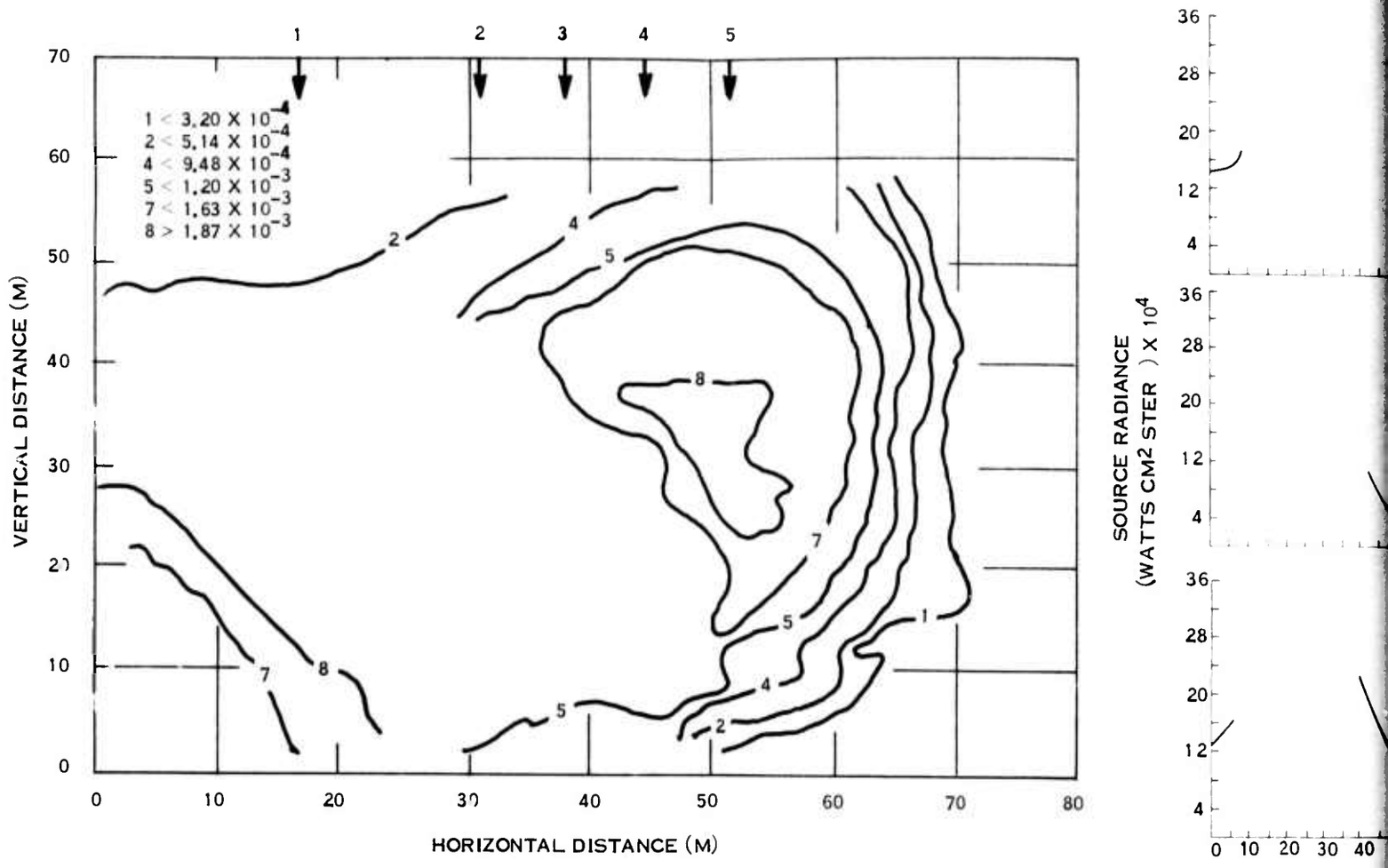

FIGURE 24. SOURCE RADIANCE - ISO-INTENSITY CONTOURS AND VERTICAL DENSITOMETER SCANS. TIME = 2.40 SECONDS.

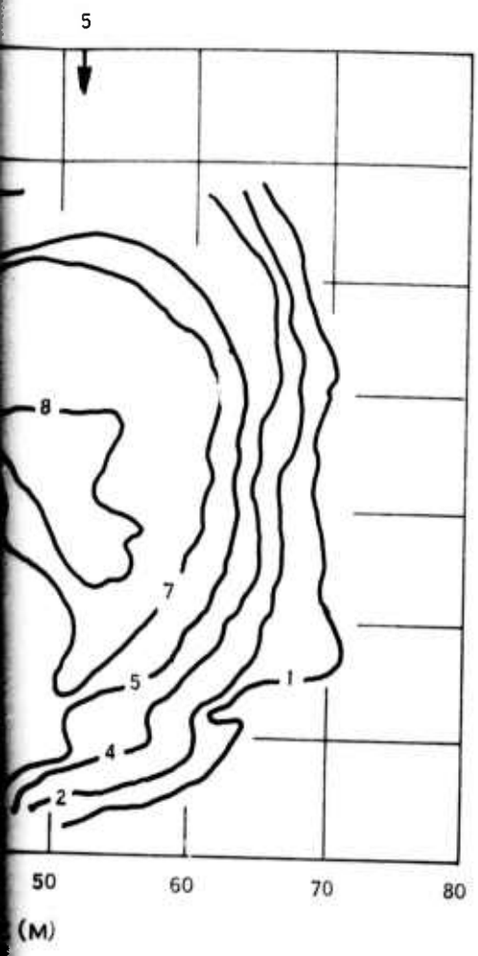

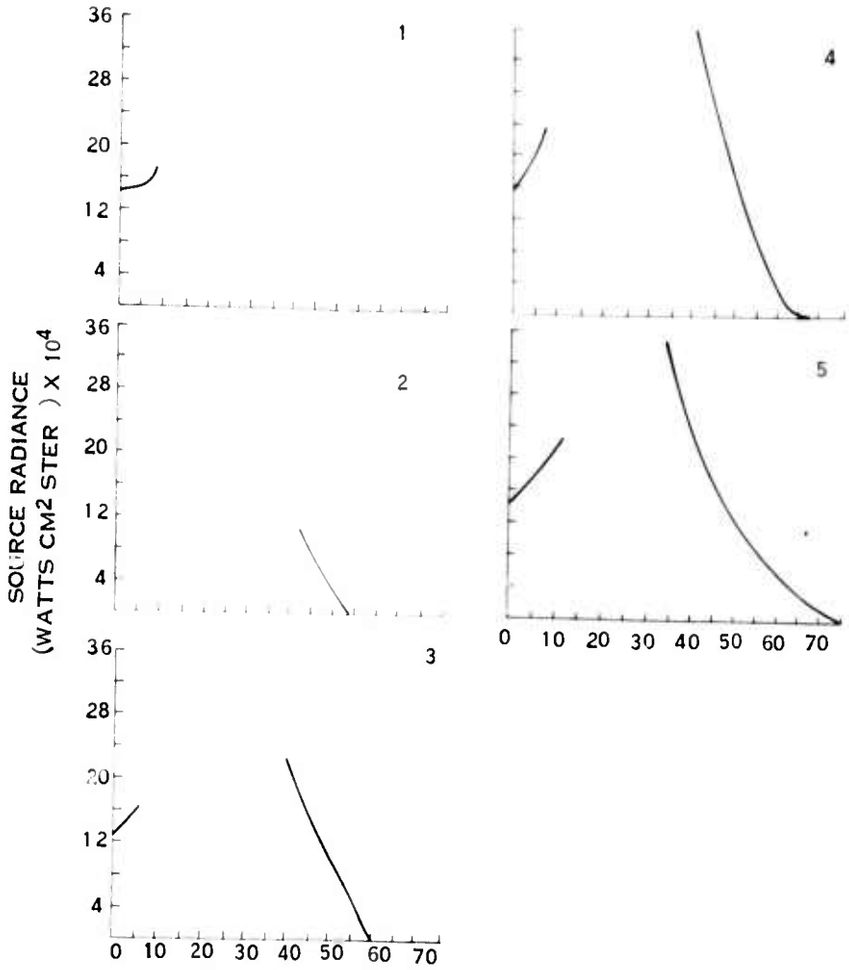

O-INTENSITY
TOMETER
DS.

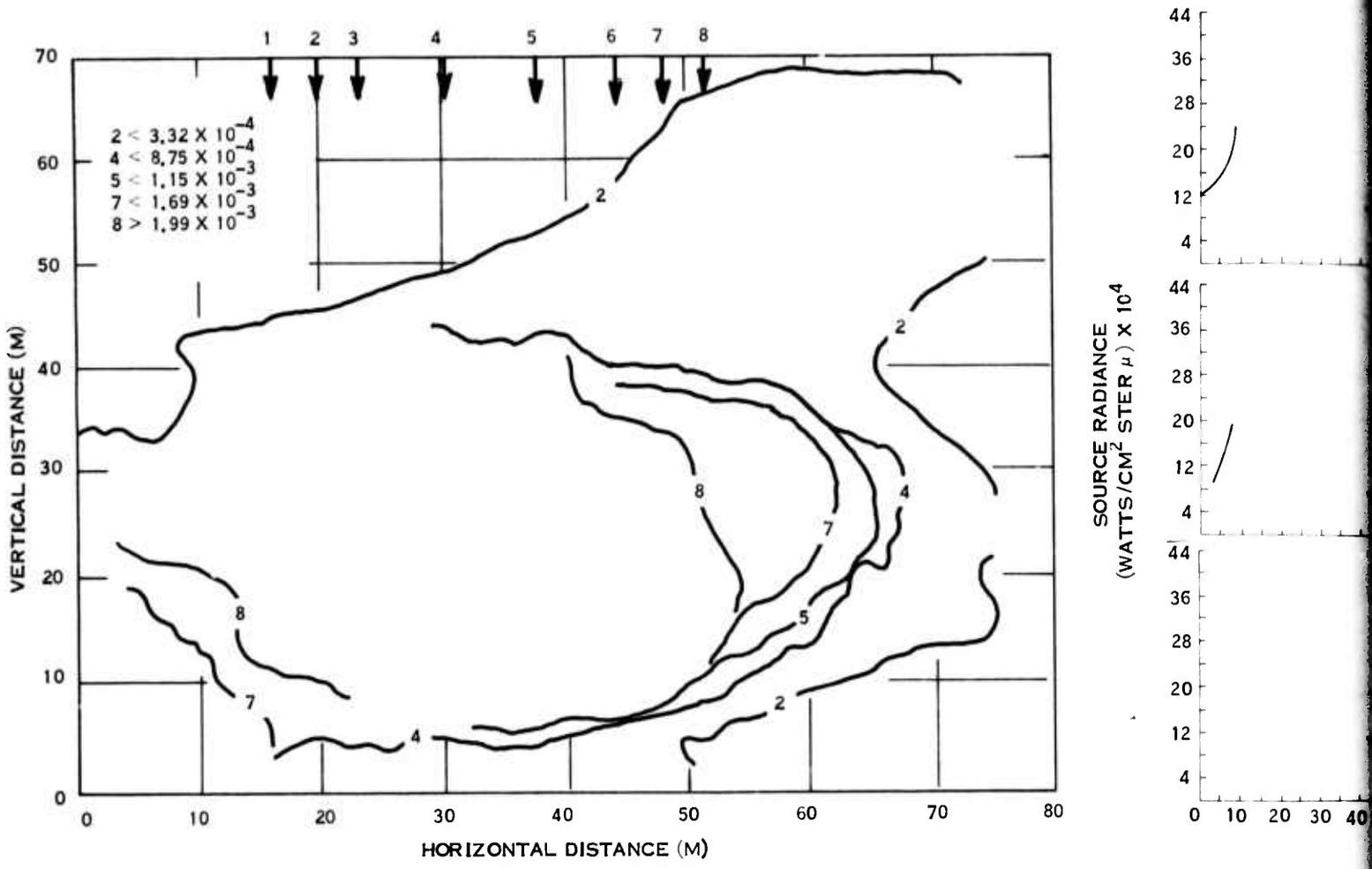

FIGURE 25. SOURCE RADIANCE - ISO-INTENSITY CONTOURS AND VERTICAL DENSITOMETER SCANS. TIME = 2.65 SECONDS.

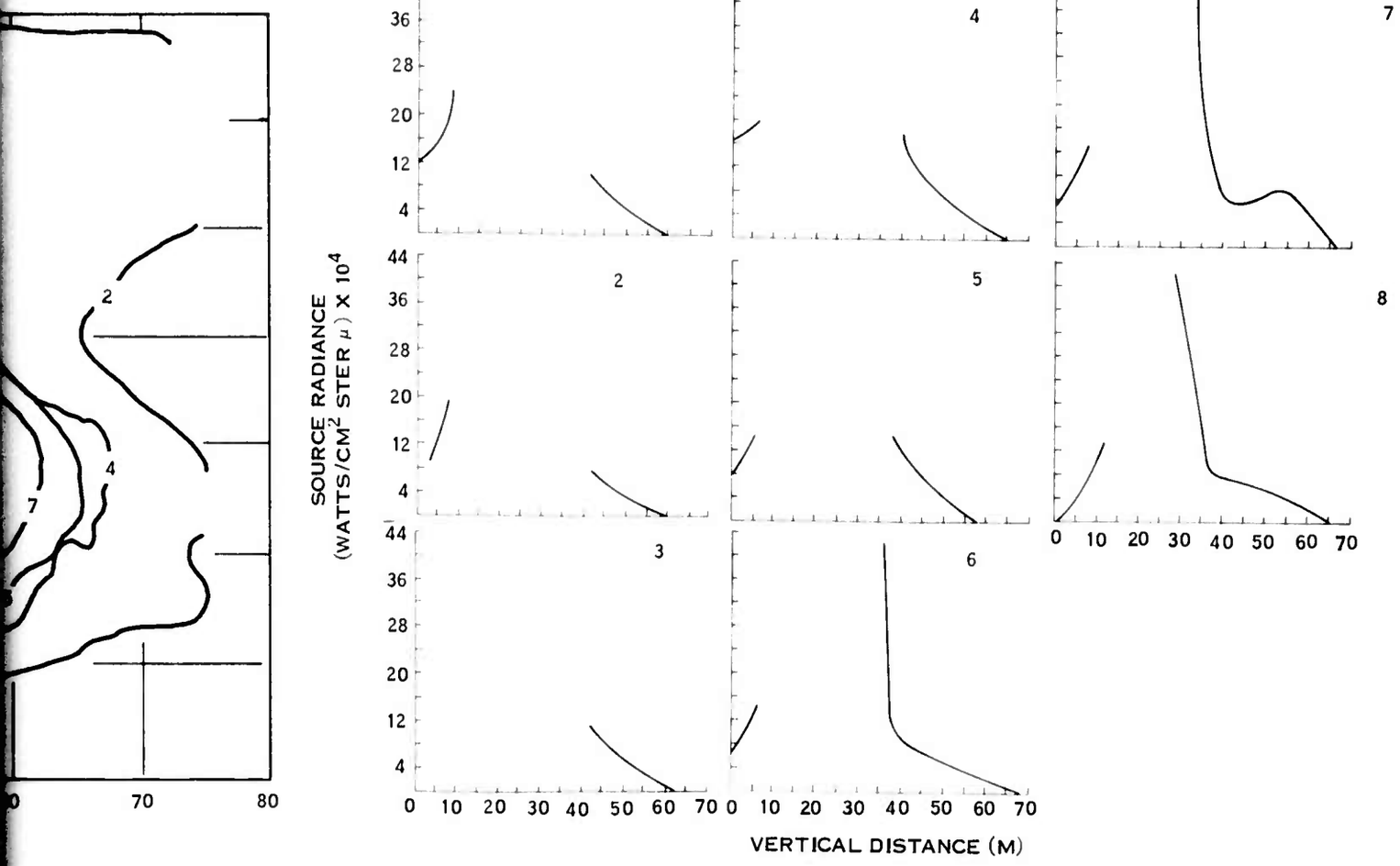
2
4
7
70
80
SOURCE RADIANCE
(WATTS/CM^2 STER μ) X 10^4
1
4
7
2
5
8
3
6
44
36
28
20
12
4
0 10 20 30 40 50 60 70
VERTICAL DISTANCE (M)

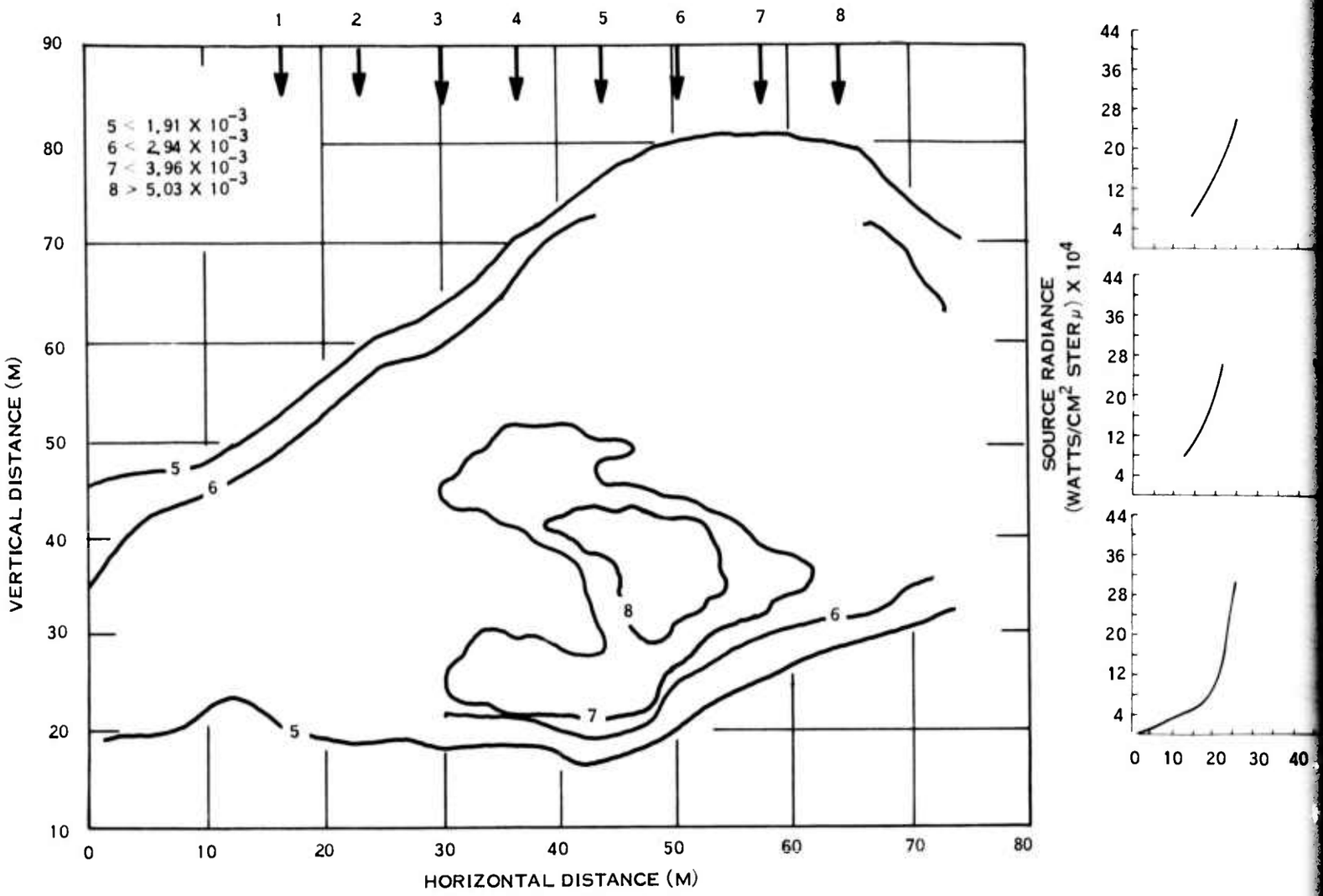

FIGURE 26. SOURCE RADIANCE - ISO-INTENSITY CONTOURS AND VERTICAL DENSITOMETER SCANS. TIME = 3.56 SECONDS.

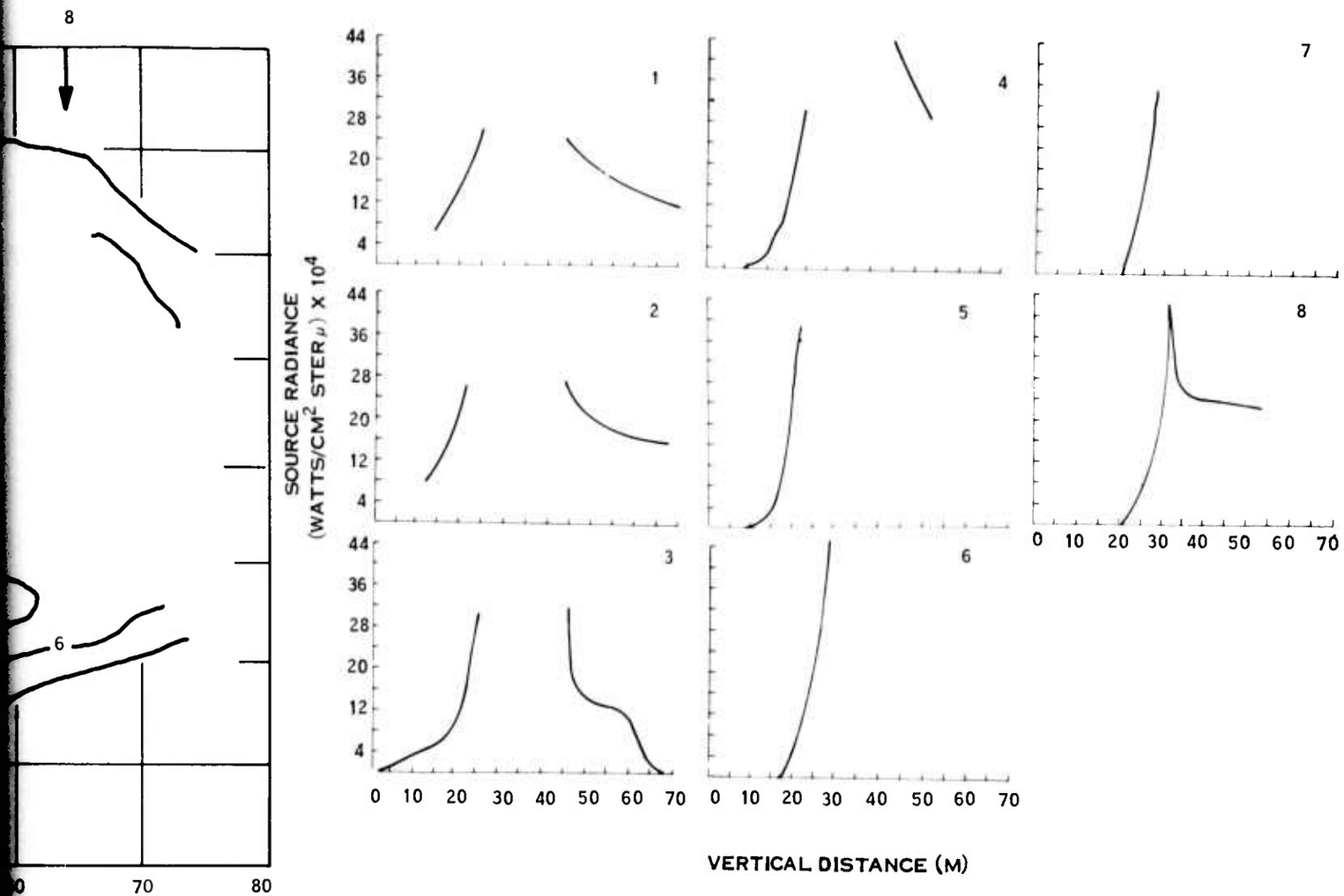
8
6
70
80
SOURCE RADIANCE
(WATTS/CM^2 STERμ) X 10^4
44
36
28
20
12
4
1
2
3
4
5
6
7
8
0 10 20 30 40 50 60 70
VERTICAL DISTANCE (M)

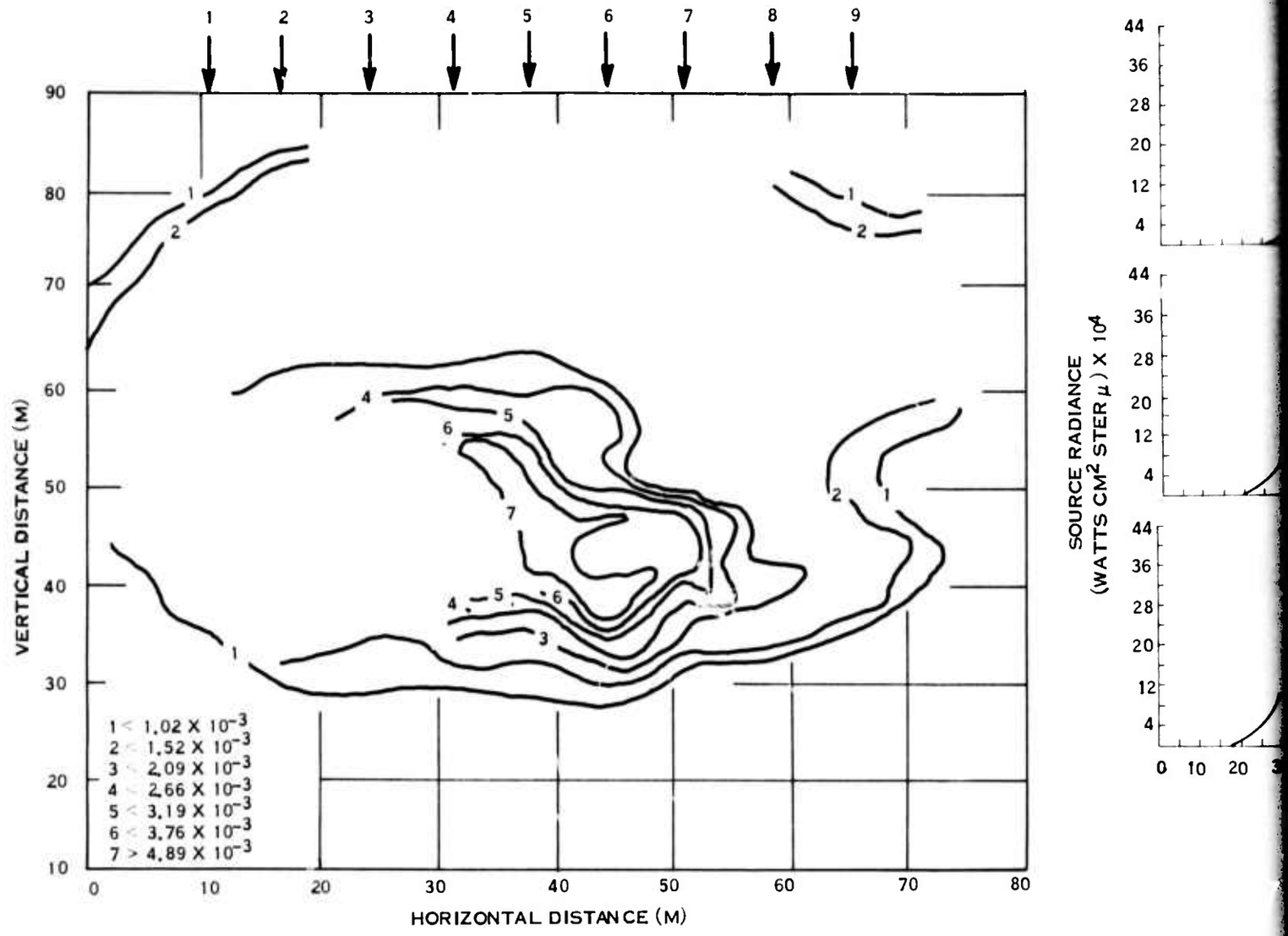

FIGURE 27. SOURCE RADIANCE - ISO-INTENSITY CONTOURS AND VERTICAL DENSITOMETER SCANS. TIME = 4.50 SECONDS.

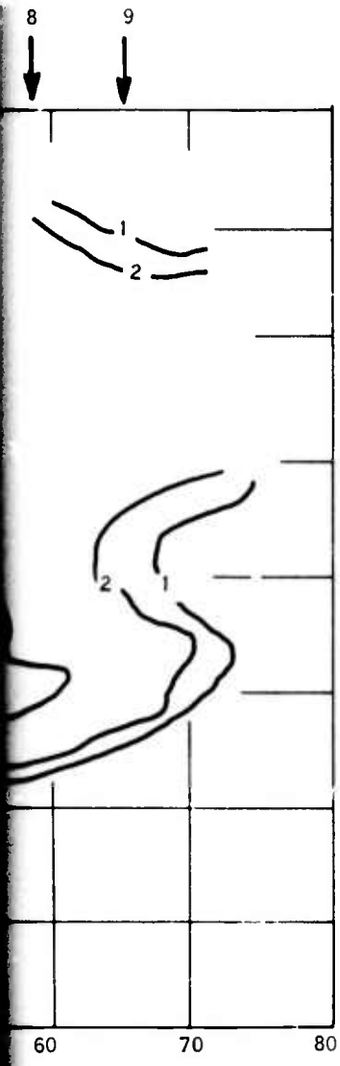
8
9
1
2
2
1
60
70
80

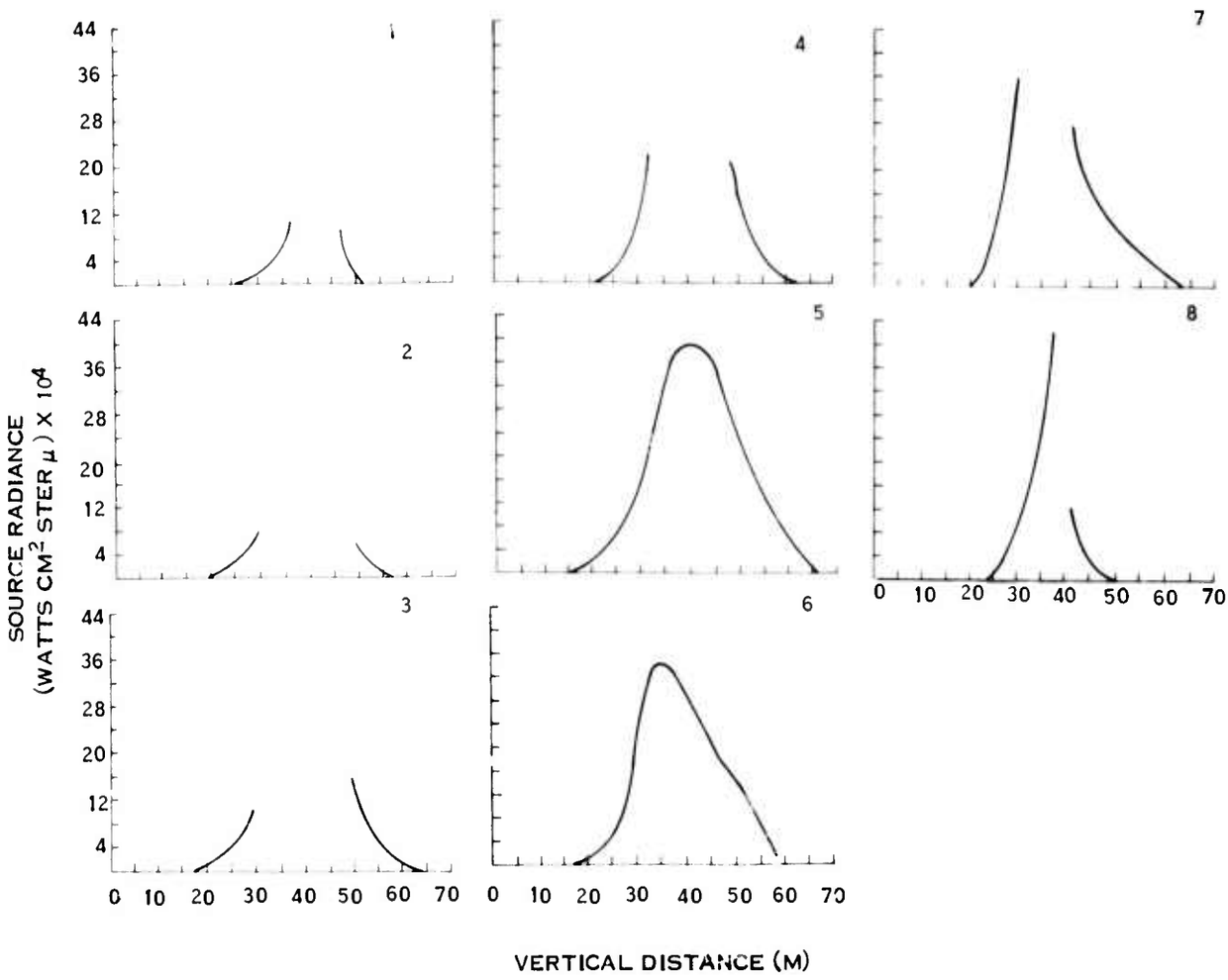
SOURCE RADIANCE
(WATTS CM^2 STER μ) X 10^4
1
4
7
2
5
8
3
6
44
36
28
20
12
4
0 10 20 30 40 50 60 70
VERTICAL DISTANCE (M)

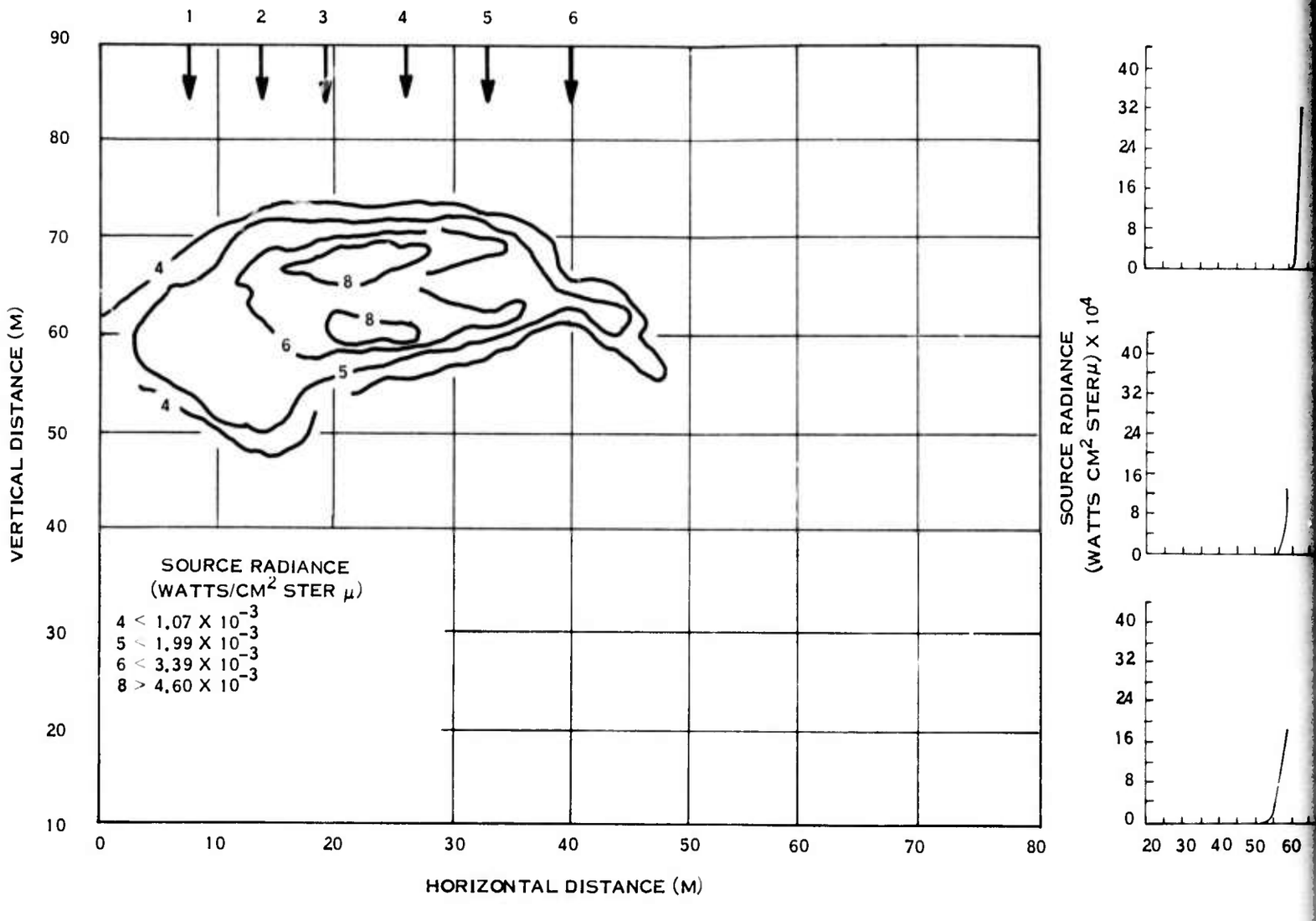

FIGURE 28. SOURCE RADIANCE - ISO-INTENSITY CONTOURS AND VERTICAL DENSITOMETER SCANS. TIME = 6.00 SECONDS.

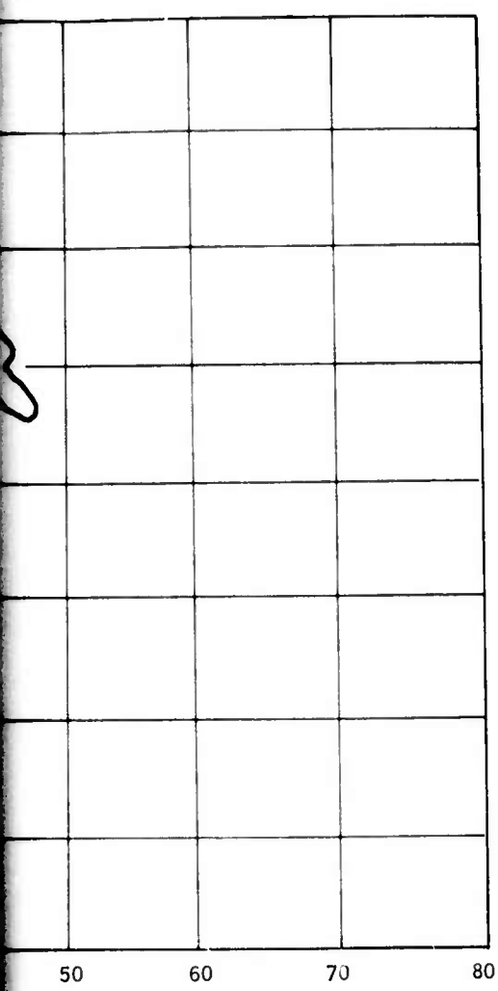

CE (M)

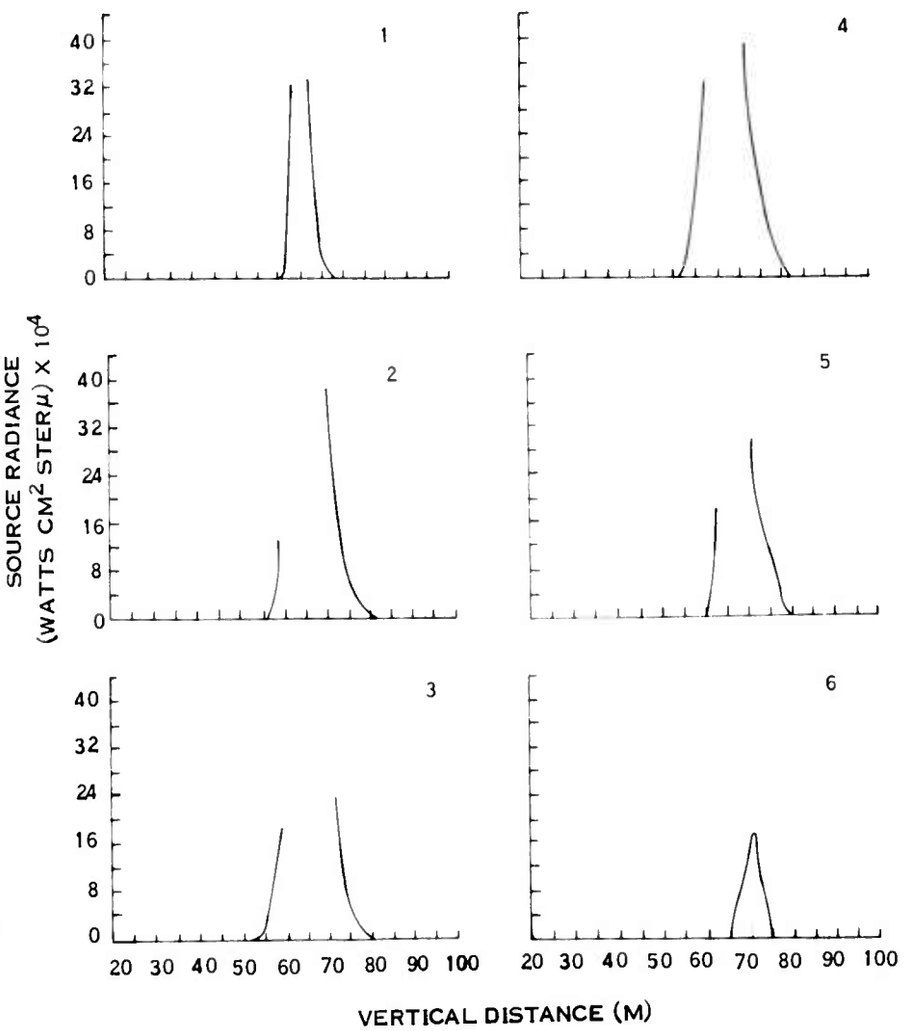

- ISO-INTENSITY
NSITOMETER
CONDS.

V. SUMMARY OF THE EXPLODING BALLOON MEASUREMENT PROGRAM

The Air Force Weapons Laboratory conducted a series of field experiments to evaluate the flow characteristics of balloon explosions. A primary diagnostic for these events was the GE operated infrared vidicon sensor system. The objective of the current program was to design the vidicon diagnostic experiment, conduct field measurements and perform an analysis of the accrued data.

Major milestones of the program have been previously documented and include:

1. Predictions of the infrared signature produced by the debris of $CO/O_2/H_2O$ and CH_4/O_2 mixtures have been made (Reference 2).
2. These predictions were used to define the optimum experimental configuration and a mission test plan was issued (working document).
3. The sensor system was assembled, checked out in the laboratory and used to conduct field measurements.
4. The data have been calibrated, examined, and recorded on film (Reference 3).

In the present report, metric information describing the flow field is presented as a function of time. This includes altitude, width, thickness, vortex diameter, vortex separation, and orientation of the explosion debris. In addition, maps of absolute source radiance have been prepared using the Image 100, an automatic image processor. These are presented as iso-intensity contours with cross-plots of intensity vs. vertical distance at various horizontal locations.

The precision of the absolute irradiance measurements was estimated as $\pm$ 10%. However, because an optics dominated retina background irradiance was subtracted to obtain the absolute source radiance, errors ranging from a factor of 2 to $\pm$ 10% are present in the reported results. A comparison with interferometer data at the same wavelength, showed that the two independent measurements of total source radiance agreed to within 50%.

REFERENCES

1. Bigoni, Robert A. and Matuska, Daniel A., "Gas Explosive Simulation Technique", Technical Report No. AFWL-TR-73-129, Air Force Weapons Laboratory, Kirtland AFB, New Mexico, May 1973. (AD

2. Alyea, Fred N. and Griffith, George A., "Predictions for Infrared Vidicon Observations of Exploding Balloons", RADC-TR-73-365, October 1973. (AD772754)

3. Alyea, Fred N., Gulatsi, Richard L., and Liebling, Gerald R., "Infrared Vidicon Observations of Exploding Balloon Events", RADC-TR-74-145, April 1974. (AD780030)

4. Sandford, Brian, AFCRL private communication, November 1974.

MISSION
of
Rome Air Development Center

RADC is the principal AFSC organization charged with planning and executing the Air Force exploratory and advanced development programs for information systems, intelligence, command, control and communications technology, products and services oriented to the needs of the USAF. Primary RADC mission areas are communications, electromagnetic guidance and control, surveillance of ground and aerospace objects, intelligence data collection and handling, information system technology, and electromagnetic reliability, maintainability and compatibility. RADC has mission responsibility as assigned by AFSC for demonstration and acquisition of selected subsystems and systems in the intelligence, mapping, charting, command, control and communications areas.